FEDERAL RESERVE BANK OF SAN FRANCISCO

WORKING PAPER SERIES

A Regime-Switching Model of the Yield Curve at the Zero Bound

Jens H.E. Christensen,
Federal Reserve Bank of San Francisco

November 2013

Working Paper 2013-34
http://www.frbsf.org/publications/economics/papers/2013/wp2013-34.pdf

The views in this paper are solely the responsibility of the authors and should not be interpreted as reflecting the views of the Federal Reserve Bank of San Francisco or the Board of Governors of the Federal Reserve System.

A Regime-Switching Model of the Yield Curve at the Zero Bound

Jens H. E. Christensen†

Abstract

This paper presents a regime-switching model of the yield curve with two states: a normal state and a zero-bound state for the case when the monetary policy target rate is at its zero lower bound for a prolonged period, as the U.S. economy has been since December 2008. The model delivers estimates of the time-varying probability of exiting the zero-bound state and can be applied to generate outcome-contingent forecasts useful for portfolio stress tests. The results show that the probability of remaining in the zero-bound state has trended upward since 2009, with notable upticks following Federal Reserve decisions to provide further monetary stimulus, whether through asset purchases or forward guidance.

JEL Classification: G12, E43, E52, E58

Keywords: term structure modeling, monetary policy, zero lower bound, arbitrage-free Nelson-Siegel model

I thank Don Kim for helpful comments. Also, I am indebted to Frank Diebold for many helpful comments and suggestions. The views in this paper are solely the responsibility of the author and should not be interpreted as reflecting the views of the Federal Reserve Bank of San Francisco or the Board of Governors of the Federal Reserve System. Finally, I thank James Gillan and Lauren Ford for excellent research assistance.

†Contact information: Federal Reserve Bank of San Francisco, 101 Market Street MS 1130, San Francisco, CA 94105, USA; phone: 1-415-974-3115; e-mail: jens.christensen@sf.frb.org.

This version: November 14, 2013.

1 Introduction

Understanding fixed-income markets is important, particularly when traditional monetary policy is at its effective zero lower bound as it has been for the United States since December 2008. Being near the zero boundary poses challenges, one of which is the asymmetry in yield movements. For bond pricing and monetary policy analysis it is critical to account for this asymmetry to accurately capture the yield dynamics near the zero boundary.

The basic premise of the analysis in this paper is that, once the monetary policy target rate hits its nominal zero bound, the dynamics of fixed-income markets change because there are limits to the downside yield movements and, more importantly, the next policy change by the central bank can only be upwards.[1] This leads me to consider a regime-switching model with a normal state and a special state that is referred to as the *zero-bound state*.

A number of papers have tried to model the asymmetry near the zero boundary and its impact on yield curve dynamics. However, most of those papers are either mainly concerned that the model dynamics not violate the zero boundary, or they adjust existing models to work specifically in the zero-bound state (Krippner 2013b and Kim and Singleton 2012 are examples of the former and latter, respectively). They typically do not model a normal and a zero-bound state jointly and the switch between the two.

To understand the features that a model should capture in the zero-bound state and to motivate the model, I first analyze the shift in the statistical properties of the U.S. Treasury yield curve since December 2008, with a particular emphasis on the variation in short-term yields. The analysis reveals that the whole yield curve switches dynamics in the zero-bound state, but the changes are particularly pronounced for yields with less than one year to maturity. As a consequence, U.S. Treasury data seem to call for a fourth factor with a unique role in the short end of the yield curve while in the zero-bound state. Based on this observation, the Treasury yield curve in the normal state is modeled with a standard three-factor term structure model, while the dynamics in the zero-bound state is augmented with a fourth factor that is a square-root process with a special role as detailed in the following.

The key characteristic of the zero-bound state in the model is that the zero bound is given a literal interpretation, that is, while in this regime the instantaneous short rate is constant at zero. To generate variation even in short-term yields, however, there is a positive chance of exiting the zero bound at any time and this is modeled by a time-varying intensity process for a Poisson point process, the first jump of which indicates the exit from the zero bound. In structure, this is similar to the modeling of default events in the reduced-form credit risk

[1] The central bank can take other actions at the zero bound such as purchasing long-term assets or provide forward guidance on how long it expects the policy target rate to remain at the zero bound, but these are all just signaling tools that do not change the fundamental fact that when the target rate is at its effective lower bound, the next rate change is up.

literature (Duffie and Singleton 1999 is an excellent example). Theoretically, the zero-bound state is considered an undesirable temporary steady state, and U.S. monetary policymakers are thought to agree, so investors should expect an exit from the zero-bound state, if at all possible. Still, how can the switch out of the zero-bound state be unpredictable at the same time as explicit or extended period forward guidance has been provided by monetary policymakers as has been the case in the United States throughout most of the time spent at the zero bound? In short, there are conditions and states of the world in which even explicit commitments regarding the zero interest rate policy would not be honored. This validates the approach to modeling the exit out of the zero-bound state. From a modeling perspective this is no different than asking how a AAA-rated firm (or a AAA-rated sovereign for that matter) can file for bankruptcy at any given time. The key point is that even though such events appear highly unlikely, they are not impossible. In the context of U.S. monetary policy, one possibility would be for the Federal Open Market Committee (FOMC) not to follow through as stated, which is not likely, but is theoretically possible and consistent with the interpretation given by the FOMC that its policy is state-contingent. Another possibility is that, as new governors are appointed and FOMC voting members rotate, the majority view on the policy committee could change.[2]

As for the normal state, the probability of switching to the zero-bound state is assumed to be so small, on the order of 0.001 or smaller, that bond investors neglect it for pricing purposes; as such this risk is not reflected in the yield curve in the normal state. The practical implication of this assumption is that bond investors cannot (and did not) foresee a switch to the zero-bound state. Furthermore, and maybe more controversial, a return to the old normal state is assumed whenever the economy leaves the zero-bound state. The motivation for this choice is simple: it is a best guess of what the yield curve dynamics will be after the economy exits the zero-bound state.[3] This choice can also be grounded with theoretical considerations. First, there is little evidence to suggest that the way investors process and price information into the Treasury yield curve has changed during the financial crisis.[4] Second, there has been no change in the way the FOMC operates and communicates its monetary policy decisions. If anything, it has become more transparent, exemplified by the

[2]The projections of future target rates first published following the January 2012 FOMC meeting do show dispersion in the anticipated appropriate stance of monetary policy among FOMC members over the committed period.

[3]Krippner (2013a) shows that the arbitrage-free Nelson-Siegel (AFNS) model used for the yield curve in the normal state can be viewed as a close approximation to any Gaussian three-factor model provided the eigenvalues corresponding to the second and third principal components are close. Given that this historically has been the case, there is little to suggest that this would not continue to hold after the exit from the zero-bound state. If so, the AFNS model structure will still deliver a very close approximation to the data, even if the yield curve dynamics obeyed an arbitrary three-factor Gaussian model.

[4]Swanson and Williams (2013) provide evidence that during 2009 and 2010, medium- and long-term Treasury yields have responded to news in much the same way as in the prior decades. This supports the model choice to keep the three factors from the normal state in the zero-bound state.

release of the explicit definition of price stability following the January 2012 FOMC meeting as an annual change of 2 percent in the price index for personal consumption expenditures. And third, the inflation process does not seem to have changed fundamentally despite its low levels in recent years. As such, the response function of the FOMC can be assumed to be constant.[5] It should be emphasized that the assumption of a return to the old normal state after the exit from the zero-bound state embodies a firm expectation that the FOMC will not raise rates prematurely, i.e., without the economy being sufficiently strong to withstand the associated tightening of financial conditions, and hence avoid the double dip scenarios Japan has experienced during its time with near zero yields. Implicitly, once the FOMC exits the zero-bound state, it is expected to stay the course until policy rates have reached more normal levels consistent with conventional monetary policy rules.

Finally, it is assumed that the transition between the two states is observed. In the empirical implementation of the model this implies that the regime switch to the zero-bound state occurs on December 16, 2008, when the FOMC decided to lock its target rate in the range from 0 to 25 basis points, which represents its effective lower bound, and this was observed by all agents in the economy.

In the empirical analysis the model is estimated on the full sample. First, and most importantly (but not surprisingly), the regime-switching model is observed to outperform a regular three-factor term structure model with no regime switch. In particular, the fit of the short-term yields is improved significantly as expected. Second, the estimated probability of remaining in the zero-bound state exhibits a time variation with upward movements around major decisions by the FOMC regarding either its large-scale asset purchase (LSAP) programs or its forward guidance for future policy during the zero-bound period. I interpret this finding as evidence of a signaling channel in the response of Treasury yields to LSAP programs, as also emphasized by Bauer and Rudebusch (2013b) and Christensen and Rudebusch (2012, henceforth CR). Third, I study the model's term premium decomposition and compare the results during the most recent zero-bound period to those from two existing dynamic term structure models of the U.S. Treasury yield curve, namely the U.S. Treasury yield model favored by CR and the Kim and Wright (2005, henceforth KW) model maintained at the Federal Reserve Board.[6] In general, the regime-switching model produces term premiums that are highly correlated with those of the existing models, but they are slightly larger on average and a bit more volatile. Still, all three models indicate that term premiums were negative and historically low during the last six months of the sample, likely as a consequence

[5]The very stable ten-year inflation forecasts from the Survey of Professional Forecasters is consistent with this view as it reflects the public's continued trust that the FOMC would counter any significant deviations in the outlook for inflation over the medium-term to ensure that the stated long-run price stability goal would be achieved.

[6]This model and its estimation are described in Kim and Orphanides (2012).

of the unconventional monetary policies pursued by the Fed. Lastly, the model delivers outcome-contingent forecasts of the future shape of the Treasury yield curve both under the assumption that the economy remains in the zero-bound state and under the assumption that the economy exits the zero-bound state before the end of the forecast horizon. I demonstrate this by making a one-year forecast of the Treasury yield curve as of the end of the sample. This is a useful tool for bond investors in creating realistic scenarios for either outcome. Another potential application could be for stress tests of a bank's portfolio.

There are two research literatures particularly relevant for the analysis in this paper. The first is the nascent, but growing literature on assessing the Fed's exit (or "liftoff" in Fed lingo) from the zero-bound state. A number of papers in this literature combine Gaussian shadow-rate models that respect the zero lower bound for nominal yields with macroeconomic variables (Bauer and Rudebusch 2013a and Wu and Xia 2013 are examples).[7] Unlike those studies, I rely solely on Treasury yields for model estimation, which allows for high frequency updates and avoids the challenging complication of determining any structural breaks between bond market functioning and real economic variables as a consequence of the zero lower bound on yields.

The second relevant literature, of course, is the vast literature on modeling the yield curve with regime switches. However, unlike that literature where, for tractable pricing, transition probabilities under the risk-neutral Q-measure are at most regime dependent (e.g., Dai et al. 2007 and Koeda 2013), the probability of exiting the zero-bound state in the model introduced in this paper is truly stochastic under both the objective and the risk-neutral probability measures. Technically, the study closest to this paper is the analysis by Piazzesi (2005), who introduced a model in which jumps in the Fed's policy rate are discrete with stochastic intensity but these jumps do not represent a switch in the dynamic structure as in the model described here.

The remainder of the paper is structured as follows. Section 2 describes how U.S. Treasury yields, short-term yields in particular, have behaved at the zero bound relative to the prior normal period. This motivates the regime-switching model introduced in Section 3. Section 4 presents the empirical results, while Section 5 describes the model's term premium decomposition and yield curve forecasts. Section 6 concludes. Appendices contain technical details on model estimation and the calculation of policy expectations and term premiums.

[7] Koeda (2013) implements a Gaussian macro-finance model of Japanese bond yields with regime-switches to analyze the time-varying probability of the Bank of Japan leaving its zero interest rate policy.

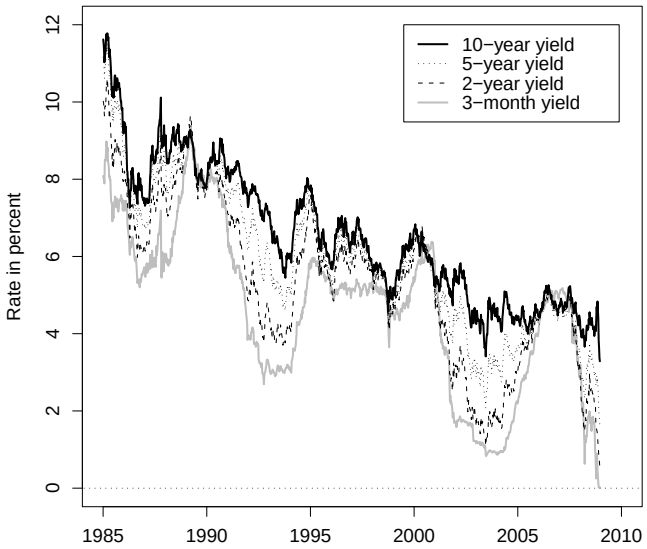

Figure 1: **U.S. Treasury Bond Yields Before December 2008.** Shown are time-series plots of U.S. zero-coupon Treasury bond yields at maturities of 3 months, 2 years, 5 years, and 10 years. The data are weekly from January 4, 1985, to December 12, 2008.

2 U.S. Treasury Yields in Normal and Zero-Bound States

The yield data used are three- and six-month yields from the H.15 data series combined with one-, two-, three-, five-, seven-, and ten-year yields from the Gürkaynak et al. (2007) database.[8] The data are continuously compounded zero-coupon yields, measured weekly (Fridays), from January 4, 1985, to December 28, 2012.

2.1 The Treasury Yield Curve in the Normal State

I start with an analysis of the subset of the sample before the FOMC first fixed the target for the overnight federal funds rate in the 0-25 basis point range, that is, before December 16, 2008, which I define as the normal state. Figure 1 shows the variation in four of the eight yield series during this period, while Table 1 reports the summary statistics for this subsample. The first observation is that the term structure is upward sloping on average. Second, short- and medium-term yields are more volatile than long-term yields.

Researchers have typically found that three factors are sufficient to model the time-variation in the cross section of U.S. Treasury bond yields (e.g., Litterman and Scheinkman,

[8]Both datasets are available online from the Board of Governors of the Federal Reserve System. See http://www.federalreserve.gov/releases/h15/ and http://www.federalreserve.gov/pubs/feds/2006/index.html.

Maturity (months)	Mean (percent)	Std. dev. (percent)	Skewness	Kurtosis
3	4.68	2.07	-0.15	2.39
6	4.87	2.10	-0.14	2.38
12	5.08	2.11	-0.14	2.35
24	5.37	2.07	-0.04	2.41
36	5.60	2.02	0.08	2.46
60	5.95	1.93	0.28	2.52
84	6.22	1.86	0.41	2.54
120	6.52	1.77	0.51	2.58

Table 1: **Summary Statistics for U.S. Treasury Bond Yields Before December 2008.** The data are weekly U.S. zero-coupon Treasury bond yields from January 4, 1985, to December 12, 2008, at 8 maturities ranging from 3 months to 10 years. There are 8×1,250 observations total.

Maturity in months	Loading on		
	First P.C.	Second P.C.	Third P.C.
3	-0.36	-0.44	0.57
6	-0.37	-0.40	0.19
12	-0.38	-0.28	-0.27
24	-0.38	-0.06	-0.47
36	-0.37	0.10	-0.39
60	-0.34	0.31	-0.08
84	-0.32	0.43	0.17
120	-0.30	0.53	0.40
% explained	94.68	5.04	0.23

Table 2: **Factor Loadings, U.S. Treasury Bond Yields Before December 2008.** In the top rows the eigenvectors corresponding to the first three principal components are shown. Put differently, they show how the bond yields at various maturities load on the first three principal components. In the final row the proportion of all bond yield variability explained by each principal component is shown. The data are weekly U.S. zero-coupon Treasury bond yields from January 4, 1985, to December 12, 2008, at eight maturities ranging from 3 months to 10 years. There are 8×1,250 observations total.

1991). Indeed, for the weekly U.S. Treasury bond yield data before mid-December 2008, 99.95% of the total variation is accounted for by three factors. Table 2 reports the eigenvectors that correspond to the first three principal components of the subsample. The first principal component accounts for 94.7% of the variation in the Treasury bond yields, and its loading across maturities is uniformly negative. Thus, like a level factor, a shock to this component changes all yields in the same direction, irrespective of maturity. The second principal component accounts for 5.0% of the variation in these data and has sizable negative loadings for the shorter maturities and sizable positive loadings for the long maturities. Thus, like a slope factor, a shock to this component steepens or flattens the yield curve. Finally, the third component, which accounts for 0.2% of the variation, has a U-shaped factor loading as a function of maturity, which is naturally interpreted as a curvature factor. This motivates the use of the Nelson and Siegel (1987) model with its level, slope, and curvature factors

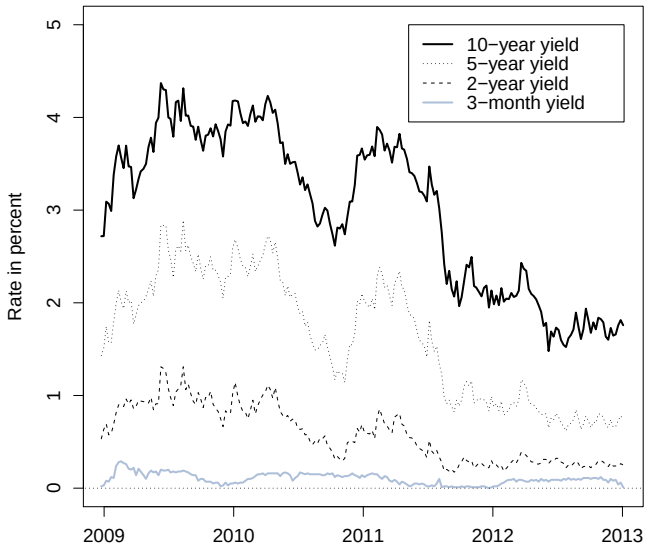

Figure 2: **U.S. Treasury Bond Yields After December 2008.** Shown are time-series plots of U.S. zero-coupon Treasury bond yields at maturities of 3 months, 2 years, 5 years, and 10 years. The data are weekly from December 19, 2008, to December 28, 2012.

for modeling the subsample of U.S. Treasury yields that represent the normal state, even though it should be noted that the estimated state variables are *not* identical to the principal component factors discussed here.[9]

2.2 The Treasury Yield Curve in the Zero-Bound State

Now, I repeat the analysis, but focus on the data since the target rate hit the zero bound in mid-December 2008. Figure 2 shows the time variation during this period for the same four yield maturities illustrated in Figure 1. A key distinguishing feature of Treasury yields in the zero-bound state is that medium- and long-term yields can vary significantly at the same time that three- and six-month yields exhibit minimal variation; this is rarely the case in the normal state. Table 3 contains the summary statistics of the yields in the zero-bound state. First, the yield curve continues to be upward sloping, and now systematically so as observed in Figure 2. However, equally important, all yields are less volatile, but obviously the short- to medium-term yields are the ones that have experienced the greatest reduction in yield volatility and are now much less volatile than their long-term counterparts. Thus, a model that accounts for both a normal state and a zero-bound state should replicate this

[9] A number of recent papers use principal components as state variables. Joslin et al. (2011) is an example.

Maturity (months)	Mean (percent)	Std. dev. (percent)	Skewness	Kurtosis
3	0.10	0.06	0.38	2.90
6	0.18	0.09	0.95	4.10
12	0.32	0.15	0.82	2.87
24	0.58	0.30	0.36	1.86
36	0.92	0.45	0.19	1.69
60	1.64	0.67	-0.03	1.58
84	2.28	0.80	-0.17	1.59
120	3.01	0.86	-0.30	1.64

Table 3: **Summary Statistics for U.S. Treasury Bond Yields After December 2008.** The data are weekly U.S. zero-coupon Treasury bond yields from December 19, 2008, to December 28, 2012, at eight maturities ranging from 3 months to 10 years. There are 8×211 observations total.

Maturity (months)	Loading on			
	First P.C.	Second P.C.	Third P.C.	Fourth P.C.
3	-0.02	-0.15	0.34	0.76
6	-0.04	-0.29	0.50	0.22
12	-0.08	-0.44	0.46	-0.37
24	-0.20	-0.53	-0.07	-0.27
36	-0.31	-0.44	-0.33	0.00
60	-0.46	-0.12	-0.35	0.29
84	-0.55	0.16	-0.05	0.14
120	-0.59	0.43	0.42	-0.26
% explained	97.84	1.64	0.43	0.07

Table 4: **Factor Loadings, U.S. Treasury Bond Yields After December 2008.** In the top rows the eigenvectors corresponding to the first three principal components are shown. Put differently, they show how the bond yields at various maturities load on the first three principal components. In the final row the proportion of all bond yield variability explained by each principal component is shown. The data are weekly U.S. zero-coupon Treasury bond yields from December 19, 2008, to December 28, 2012, at eight maturities ranging from 3 months to 10 years. There are 8×211 observations total.

pattern. Furthermore, it should account for the change in the level of interest rates that occur when we move to the zero-bound state.

As in the previous section, I use principal components analysis to better understand the factors driving the variation in the yield curve in the zero-bound state. The result is reported in Table 4. The first three components explain 99.91 percent of the variation, and the loadings on the corresponding eigenvectors across yield maturities have changed though they still reflect a pattern of level, slope, and curvature. Importantly, it now appears that a fourth factor explains 0.1% of the variation in yields in the zero-bound state and is needed to fully account for the yield dynamics in that state. Furthermore, the loadings on the fourth factor do not have a structure that matches the pattern of either level, slope, or curvature. It has its biggest loading in the very short end of the yield curve (more than twice the size of any of the other loadings). At the same time, the first and second principal components

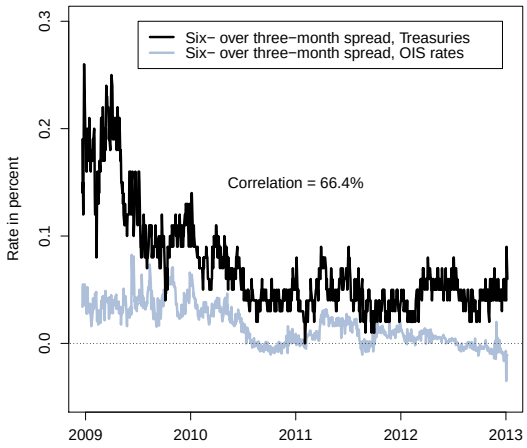

(a) Spread of six- over three-month yields.

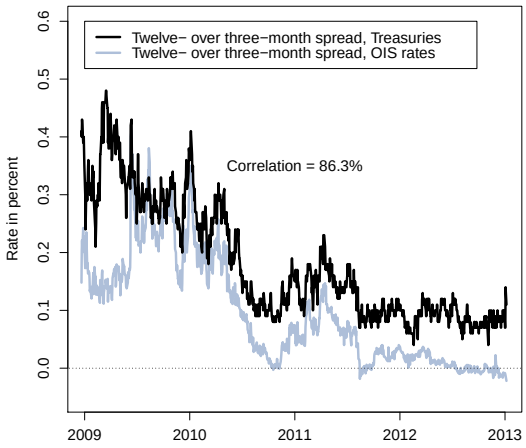

(b) Spread of twelve- over three-month yields.

Figure 3: **Short-Term Interest Rate Spreads After December 2008.** Panel (a) shows the spreads of six-month over three-month yields for Treasuries and OIS contracts. Panel (b) shows the corresponding spreads of twelve-month over three-month yields. The data are daily from December 16, 2008, to December 31, 2012.

have seen a significant reduction in their loadings on the short-term yields. Thus, it seems that the additional fourth factor is mainly operating in the short end of the curve, where we would expect the biggest changes to the yield curve dynamics to occur when the economy enters the zero-bound state. A good model should account for this pattern in addition to the other stylized facts described above.

2.3 Short Rates in the Zero-Bound State

To get a better sense of the properties of the fourth factor that must be incorporated into the standard three-factor dynamic term structure model, I study the variation in the short end of the U.S. Treasury yield curve in greater detail.

Figure 3(a) shows the variation in the six- over three-month yield spreads from Treasuries and overnight interest swap (OIS) rates, while Figure 3(b) shows the variation in the corresponding twelve- over three-month yield spreads. With correlations in the yield spreads from the two curves of 66.4 percent for the six- over three-month spreads and 86.3 percent for the twelve- over three-month yield spreads, it is evident that the specific type of yield data used does not seem to matter for the type of inference we want to make here.[10]

[10]It should be noted that if OIS rates are used in model estimation, a parsimonious term structure model could have some difficulty replicating the occasional negative slope of the short end of the OIS curve, which does not occur in the Treasury data sample. However, these slight inversions are likely the result of microstructure noise rather than investor expectations.

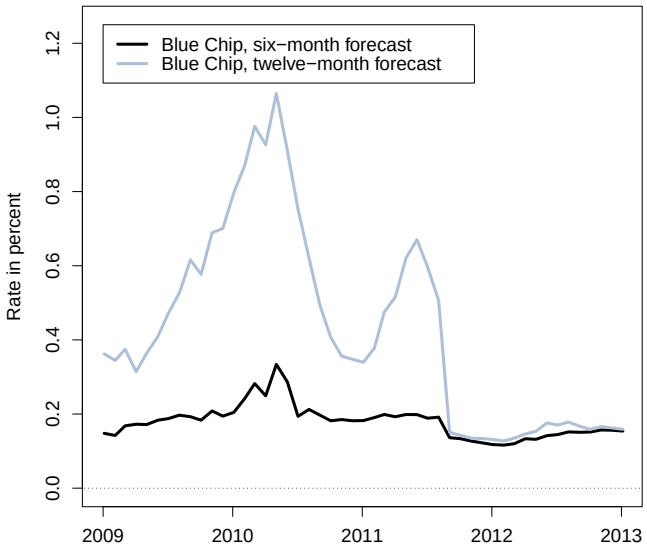

Figure 4: **Blue Chip Federal Funds Rate Survey Forecasts After December 2008.** The Blue Chip survey forecasts refer to the median of the forecasts for the end of each quarter. As a consequence, linear interpolation is used to generate forecasts with constant horizons of 6 and 12 months. The data are monthly from January 1, 2009, to January 1, 2013.

Throughout 2011-2012, surveys of primary dealers conducted by the New York Fed indicate that there were effectively no expectations of exiting the zero-bound state within the subsequent six- to twelve-month period.[11] Similar low expectations for near-term future monetary policy are reflected in the monthly Blue Chip survey of professional forecasters shown in Figure 4. Thus, the fairly sizable variation in the short-term slope of the yield curve is likely *not* to reflect any material changes in the *expected* future path of monetary policy the following six to twelve months. However, they may well reflect variation in the *uncertainty* about the expected path for future monetary policy over that time horizon and, hence, affect the term premium component of bond yields.

Figure 5(a) reveals notable variation in the six- over three-month spreads of rates on federal funds and eurodollar futures contracts, while Figure 5(b) reveals even larger variation in the twelve- over three-month spreads of the futures rates. Combined with the observations above, this is evidence that term premiums are likely to be as large and volatile near the zero bound as they are in the normal state.[12] The regime-switching model introduced in the

[11] The questions and responses from the New York Fed's survey of primary dealers are available at: http://www.newyorkfed.org/markets/primarydealer_survey_questions.html.

[12] Piazzesi and Swanson (2008) provide evidence of large and time-varying risk premiums in the rates of federal funds futures contracts in the normal pre-crisis period.

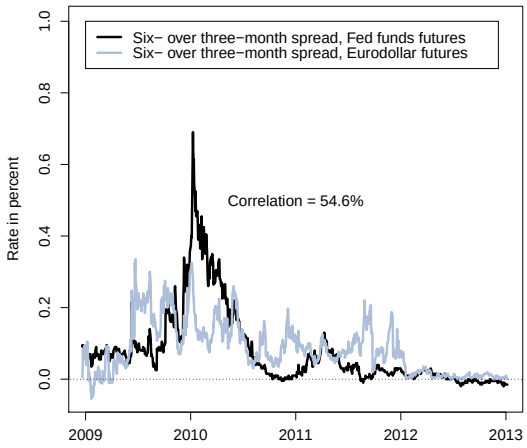

(a) Spread of six- over three-month futures.

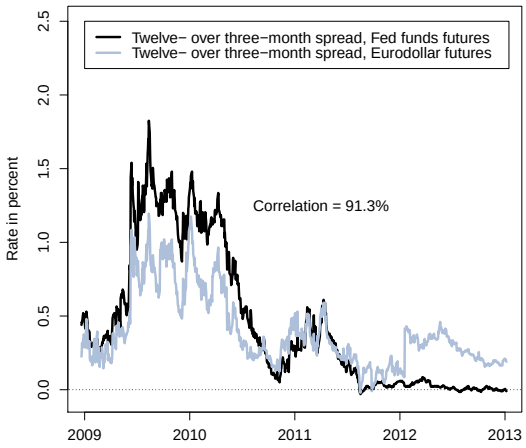

(b) Spread of twelve- over three-month futures.

Figure 5: **Spreads of Short-Term Futures Rates After December 2008.** Panel (a) shows the spreads of six-month over three-month rates on federal funds and Eurodollar futures contracts. Panel (b) shows the corresponding spreads of twelve-month over three-month futures rates. The data are daily from December 16, 2008, to December 31, 2012.

following section accommodates this aspect of the data by letting the added fourth factor be a square-root process that can generate the kind of stochastic short-term yield volatility seen in Figures 3 and 5, even though the instantaneous risk-free rate is constant at zero. Furthermore, it is important to emphasize that the objective is to create a model that accurately describes the Treasury yield curve before it reaches the zero bound, while at the zero bound, and after the exit from the zero bound.

3 Model Description

This section describes the regime-switching model studied in the remainder of the paper.

In the normal state, the yield curve is characterized by its usual level, slope, and curvature factor, here denoted (L_t, S_t, C_t), which are modeled using the arbitrage-free Nelson-Siegel (AFNS) model introduced in Christensen et al. (CDR, 2011).[13] To preserve the Nelson-Siegel factor loading structure in the yield function, the instantaneous risk-free rate is defined as:

$$r_t = L_t + S_t.$$

Furthermore, the risk-neutral (or Q-) dynamics of the state variables are given by the following

[13] See Diebold and Rudebusch (2013) for a comprehensive presentation of related applications of the AFNS model.

system of stochastic differential equations:[14]

$$\begin{pmatrix} dL_t \\ dS_t \\ dC_t \end{pmatrix} = \begin{pmatrix} 0 & 0 & 0 \\ 0 & -\lambda & \lambda \\ 0 & 0 & -\lambda \end{pmatrix} \begin{pmatrix} L_t \\ S_t \\ C_t \end{pmatrix} dt + \Sigma \begin{pmatrix} dW_t^{L,Q} \\ dW_t^{S,Q} \\ dW_t^{C,Q} \end{pmatrix},$$

where Σ is the constant covariance (or volatility) matrix.[15] Based on this specification of the Q-dynamics, zero coupon bond yields in the normal state preserve the popular Nelson and Siegel (1987) factor loading structure as

$$y_t^N(\tau) = L_t + \left(\frac{1-e^{-\lambda\tau}}{\lambda\tau}\right) S_t + \left(\frac{1-e^{-\lambda\tau}}{\lambda\tau} - e^{-\lambda\tau}\right) C_t - \frac{A^N(\tau)}{\tau}, \tag{1}$$

where $A^N(\tau)/\tau$ is a maturity-dependent yield-adjustment term that applies in the normal state.[16]

The zero-bound state has two salient features. First, the instantaneous short rate is assumed constant and fixed at zero, to be consistent with the data.[17] Second, it is assumed that there is an additional state variable that drives the variation in the intensity process for the Poisson jump process that indicates the switch out of the zero-bound state. This process is denoted η_t and is assumed to follow a square-root process to preserve strict positivity:

$$d\eta_t = \kappa_\eta^Q(\theta_\eta^Q - \eta_t)dt + \sigma_\eta\sqrt{\eta_t}dW_t^{\eta,Q}.$$

The implication of this modeling approach is that the switch from the zero-bound state back to the normal state is unpredictable, even in the days before the actual announcement. This modeling choice can be defended in two ways. First, from December 2008 until August 2011, the FOMC only used "extended period" language so it was left to anybody's guess as to what defined an extended period. Thus, during this period, the exact switch date could not be foreseen. Second, after August 2011 when explicit forward guidance was introduced, it was still uncertain whether the zero-bound period would extend beyond the explicit future date or even whether the FOMC would change its mind before reaching that date. Thus, in

[14] As discussed in CDR, with a unit root in the level factor under the pricing probability measure, the model is not arbitrage-free with an unbounded horizon; therefore, as is often done in theoretical discussions, an arbitrary maximum horizon is imposed.

[15] As per CDR, Σ is a diagonal matrix, and θ^Q is set to zero without loss of generality.

[16] CDR provide the analytical formula for $A^N(\tau)/\tau$.

[17] In the daily H.15 database through 2012 (of which I use a weekly subsample), the zero boundary is *never* violated. The one-month yield is 0 on 40 dates, the three-month yield is 0 on 7 dates, while the six-month yield never goes below 2 basis points. Furthermore, since late 2008, the spread between the six- and three-month yields is always positive except for a single day, January 28, 2011, when it was zero. Thus, with three- and six-month yields less than 10 basis points and the yield curve steep for much of the time spent in the zero-bound state, the choice of zero for the short rate appears to be a reasonable assumption, if not outright the true value.

reality, it was never completely certain when and how the FOMC would exit the zero-bound state and, as shown by Duffie and Lando (2001), with this kind of uncertainty surrounding what might otherwise be a predictable event, it is theoretically consistent to model it as an unpredictable event with a stochastic intensity process that reflects the time-varying chance of exiting the zero-bound state at any given time.

Since the principal components decomposition of the Treasury yield curve since December 19, 2008, shown in Table 4 continues to reflect a structure with level, slope, and curvature, the dynamics of the three regular state variables are assumed not to change when the economy switches to the zero-bound state. As a consequence, the dynamics of the state variables under the pricing Q-measure in the zero-bound state are assumed to be driven by the following system of stochastic differential equations:

$$\begin{pmatrix} dL_t \\ dS_t \\ dC_t \\ d\eta_t \end{pmatrix} = \begin{pmatrix} 0 & 0 & 0 & 0 \\ 0 & \lambda & -\lambda & 0 \\ 0 & 0 & \lambda & 0 \\ 0 & 0 & 0 & \kappa_\eta^Q \end{pmatrix} \left[\begin{pmatrix} 0 \\ 0 \\ 0 \\ \theta_\eta^Q \end{pmatrix} - \begin{pmatrix} L_t \\ S_t \\ C_t \\ \eta_t \end{pmatrix} \right] dt + \begin{pmatrix} \sigma_L & 0 & 0 & 0 \\ 0 & \sigma_S & 0 & 0 \\ 0 & 0 & \sigma_C & 0 \\ 0 & 0 & 0 & \sigma_\eta \end{pmatrix} \begin{pmatrix} \sqrt{1} & 0 & 0 & 0 \\ 0 & \sqrt{1} & 0 & 0 \\ 0 & 0 & \sqrt{1} & 0 \\ 0 & 0 & 0 & \sqrt{\eta_t} \end{pmatrix} \begin{pmatrix} dW_t^{L,Q} \\ dW_t^{S,Q} \\ dW_t^{C,Q} \\ dW_t^{\eta,Q} \end{pmatrix}.$$

In the zero-bound state, zero coupon bond prices are calculated as follows:

$$\begin{aligned} P^Z(t,T) &= E_t^Q\left[e^{-\int_t^T r_u du}\right] \\ &= E_t^Q\left[\mathbf{1}_{\{\text{In } Z \text{ state at } T\}} + \int_t^T \mathbf{1}_{\{\text{Exit } Z \text{ state at } s\}} e^{-\int_s^T r_u du} ds\right] \\ &= E_t^Q\left[e^{-\int_t^T \eta_u du}\right] + E_t^Q\left[\int_t^T \eta_s e^{-\int_t^s \eta_u du} e^{-\int_s^T r_u du} ds\right] \\ &= E_t^Q\left[e^{-\int_t^T \eta_u du}\right] + \int_t^T E_t^Q\left[\eta_s e^{-\int_t^s \eta_u du} E_s^Q(e^{-\int_s^T r_u du})\right] ds \\ &= E_t^Q\left[e^{-\int_t^T \eta_u du}\right] \\ &\quad + \int_t^T E_t^Q\left[\eta_s e^{-\int_t^s \eta_u du} e^{A^N(s,T)+B_L^N(s,T)L_s+B_S^N(s,T)S_s+B_C^N(s,T)C_s}\right] ds. \end{aligned}$$

The first term is the probability of remaining in the zero-bound state beyond time T in which case discounting is done throughout at zero interest. The second term is the cumulative probability of exiting the zero-bound state prior to time T multiplied by risk-neutral discounting using the normal-state dynamics of the short rate over the remaining time until T.

The formulas needed to calculate the above expectations are provided in the following proposition.[18]

Proposition 1:

In the zero-bound state, zero coupon bond prices are calculated as follows:

$$P^Z(t,T) = E_t^Q\left[e^{-\int_t^T \eta_u du}\right] + \int_t^T E_t^Q\left[\eta_s e^{-\int_t^s \eta_u du} e^{A^N(s,T)+B_L^N(s,T)L_s+B_S^N(s,T)S_s+B_C^N(s,T)C_s}\right] ds,$$

where

$$E_t^Q\left[e^{-\int_t^T \eta_u du}\right] = \exp\Big(A_\eta(t,T) + B_\eta(t,T)\eta_t\Big), \tag{2}$$

$$A_\eta(t,T) = \frac{2\kappa_\eta^Q\theta_\eta^Q}{\sigma_\eta^2}\ln\left[\frac{2\phi_\eta e^{\frac{1}{2}(\phi_\eta+\kappa_\eta^Q)(T-t)}}{2\phi_\eta + (\phi_\eta+\kappa_\eta^Q)(e^{\phi_\eta(T-t)}-1)}\right], \tag{3}$$

$$B_\eta(t,T) = \frac{-2(e^{\phi_\eta(T-t)}-1)}{2\phi_\eta + (\phi_\eta+\kappa_\eta^Q)[e^{\phi_\eta(T-t)}-1]}, \tag{4}$$

and

$$\begin{aligned} & E_t^Q\left[\eta_s e^{-\int_t^s \eta_u du} e^{A^N(s,T)+B^L(s,T)L_s+B^S(s,T)S_s+B^C(s,T)C_s}\right] \\ = \; & \exp\Big(A^Z(t,s,T) + B_L^Z(t,s,T)L_t + B_S^Z(t,s,T)S_t + B_C^Z(t,s,T)C_t + B_\eta^Z(t,s,T)\eta_t\Big) \\ & \times\Big[C^Z(t,s,T) + D_\eta^Z(t,s,T)\eta_t\Big] \end{aligned}$$

[18] The calculations leading to the formulas in Proposition 1 are available upon request.

with

$$
\begin{aligned}
A^Z(t,s,T) &= \overline{A}^N(s,T) + \frac{\sigma_L^2}{2}\overline{B}_L^N(s,T)^2(s-t) + \frac{\sigma_S^2}{2}\overline{B}_S^N(s,T)^2\frac{1-e^{-\lambda(s-t)}}{\lambda} \\
&\quad +\sigma_C^2\overline{B}_C^N(s,T)^2\frac{1-e^{-2\lambda(s-t)}}{4\lambda} \\
&\quad +\frac{\sigma_C^2}{2}\overline{B}_C^N(s,T)^2\Big[-\frac{1}{2}\lambda(s-t)^2e^{-2\lambda(s-t)} - \frac{1}{2}(s-t)e^{-2\lambda(s-t)} + \frac{1-e^{-2\lambda(s-t)}}{4\lambda}\Big] \\
&\quad +\sigma_C^2\lambda\overline{B}_S^N(s,T)\overline{B}_C^N(s,T)\Big[-\frac{1}{2\lambda}(s-t)e^{-2\lambda(s-t)} + \frac{1-e^{-2\lambda(s-t)}}{4\lambda^2}\Big] \\
&\quad +\frac{2\kappa_\eta^Q\theta_\eta^Q}{\sigma_\eta^2}\ln\left[\frac{2\phi_\eta e^{\frac{1}{2}(\phi_\eta+\kappa_\eta^Q)(s-t)}}{2\phi_\eta + (\phi_\eta+\kappa_\eta^Q)(e^{\phi_\eta(s-t)}-1)}\right], \\
B_L^Z(t,s,T) &= \overline{B}_L^N(s,T), \\
B_S^Z(t,s,T) &= e^{-\lambda(s-t)}\overline{B}_S^N(s,T), \\
B_C^Z(t,s,T) &= e^{-\lambda(s-t)}\overline{B}_C^N(s,T) + \lambda(s-t)e^{-\lambda(s-t)}\overline{B}_S^N(s,T), \\
B_\eta^Z(t,s,T) &= \frac{-2(e^{\phi_\eta(s-t)}-1)}{2\phi_\eta + (\phi_\eta+\kappa_\eta^Q)[e^{\phi_\eta(s-t)}-1]}, \\
C^Z(t,s,T) &= \frac{2\kappa_\eta^Q\theta_\eta^Q\overline{D}_\eta(s,T)(e^{\phi_\eta(s-t)}-1)}{2\phi_\eta + (\phi_\eta+\kappa_\eta^Q)(e^{\phi_\eta(s-t)}-1)}, \\
D_\eta^Z(t,s,T) &= \frac{4\phi_\eta^2 e^{\phi_\eta(s-t)}\overline{D}_\eta(s,T)}{\big[2\phi_\eta + (\phi_\eta+\kappa_\eta^Q)(e^{\phi_\eta(s-t)}-1)\big]^2}.
\end{aligned}
$$

Finally, the boundary values in the formulas above are:

$$
\begin{aligned}
\overline{A}^N(s,T) &= \sigma_L^2\frac{(T-s)^3}{6} + \sigma_S^2\Big[\frac{1}{2\lambda^2}(T-s) - \frac{1}{\lambda^3}(1-e^{-\lambda(T-s)}) + \frac{1}{4\lambda^3}(1-e^{-2\lambda(T-s)})\Big] \\
&\quad +\sigma_C^2\Big[\frac{1}{2\lambda^2}(T-s) + \frac{1}{\lambda^2}(T-s)e^{-\lambda(T-s)} - \frac{1}{4\lambda}(T-s)^2e^{-2\lambda(T-s)} \\
&\qquad -\frac{3}{4\lambda^2}(T-s)e^{-2\lambda(T-s)} - \frac{2}{\lambda^3}(1-e^{-\lambda(T-s)}) + \frac{5}{8\lambda^3}(1-e^{-2\lambda(T-s)})\Big], \\
\overline{B}_L^N(s,T) &= -(T-s), \\
\overline{B}_S^N(s,T) &= -\frac{1-e^{-\lambda(T-s)}}{\lambda}, \\
\overline{B}_C^N(s,T) &= (T-s)e^{-\lambda(T-s)} - \frac{1-e^{-\lambda(T-s)}}{\lambda}, \\
\overline{D}_\eta(s,T) &= 1.
\end{aligned}
$$

Throughout it holds that

$$\phi_\eta = \sqrt{(\kappa_\eta^Q)^2 + 2\sigma_\eta^2}.$$

It is noted that zero coupon bond prices in both regimes are known in analytical form

(up to the calculation of a single integral in the maturity dimension), which facilitates the empirical implementation of the model. Also, applying the formulas in Proposition 1, zero coupon bond yields in the zero-bound state are easily calculated as

$$y^Z(t,T) = -\frac{1}{T-t}\ln P^Z(t,T). \tag{5}$$

To complete the model, the risk premium structure that provides the connection between the pricing dynamics described above and the real-world dynamics of the state variables needs to be specified. Using the extended affine risk premiums introduced in Cheridito et al. (2007), the maximally flexible specification of the model has P-dynamics given by

$$\begin{pmatrix} dL_t \\ dS_t \\ dC_t \\ d\eta_t \end{pmatrix} = \begin{pmatrix} \kappa^P_{11} & \kappa^P_{12} & \kappa^P_{13} & \kappa^P_{14} \\ \kappa^P_{21} & \kappa^P_{22} & \kappa^P_{23} & \kappa^P_{24} \\ \kappa^P_{31} & \kappa^P_{32} & \kappa^P_{33} & \kappa^P_{34} \\ 0 & 0 & 0 & \kappa^P_{44} \end{pmatrix} \left[\begin{pmatrix} \theta^P_1 \\ \theta^P_2 \\ \theta^P_3 \\ \theta^P_4 \end{pmatrix} - \begin{pmatrix} L_t \\ S_t \\ C_t \\ \eta_t \end{pmatrix} \right] dt$$
$$+ \begin{pmatrix} \sigma_L & 0 & 0 & 0 \\ 0 & \sigma_S & 0 & 0 \\ 0 & 0 & \sigma_C & 0 \\ 0 & 0 & 0 & \sigma_\eta \end{pmatrix} \begin{pmatrix} \sqrt{1} & 0 & 0 & 0 \\ 0 & \sqrt{1} & 0 & 0 \\ 0 & 0 & \sqrt{1} & 0 \\ 0 & 0 & 0 & \sqrt{\eta_t} \end{pmatrix} \begin{pmatrix} dW^{L,P}_t \\ dW^{S,P}_t \\ dW^{C,P}_t \\ dW^{\eta,P}_t \end{pmatrix}.$$

Similar to the approach for the Q-dynamics used for pricing, the P-dynamics of the level, slope, and curvature are assumed to remain the same throughout. However, a switch in the P-dynamics of the first three factors, when in the zero-bound state, can easily be incorporated if deemed appropriate.[19]

Finally, the model estimation is based on the Kalman filter and described in Appendix A.

4 Results

In this section, I first discuss the regime-switching model selection and fit, contrasting the results to those from a standard three-factor AFNS model. Second, I document the regime-switching model's ability to match the change in yield volatility near the zero lower bound. Finally, I analyze the model's assessment of the time-varying likelihood of exiting the zero-bound state in detail.

[19] The practical problem in imposing a regime switch on the upper three-dimensional part of K^P, θ^P, and Σ is twofold. First, it increases the number of parameters significantly. Second, and more importantly, there is only a short sample to identify these additional parameters from, which prevents efficient estimation.

Alternative specifications	Goodness-of-fit statistics				
	$\log L$	k	p-value	AIC	BIC
(1) Unrestricted K^P	67,660.26	40	n.a.	-135,240.5	-135,029.0
(2) $\kappa^P_{31} = 0$	67,660.09	39	0.5598	-135,242.2	-135,036.0
(3) $\kappa^P_{31} = \kappa^P_{32} = 0$	67,660.04	38	0.7518	-135,244.1	-135,043.2
(4) $\kappa^P_{31} = \kappa^P_{32} = \kappa^P_{12} = 0$	67,659.57	37	0.3323	-135,245.1	-135,049.5
(5) $\kappa^P_{31} = \ldots = \kappa^P_{14} = 0$	67,658.84	36	0.2269	**-135,245.7**	-135,055.4
(6) $\kappa^P_{31} = \ldots = \kappa^P_{21} = 0$	67,657.64	35	0.1213	-135,245.3	**-135,060.2**
(7) $\kappa^P_{31} = \ldots = \kappa^P_{34} = 0$	67,650.36	34	0.0001	-135,232.7	-135,053.0
(8) $\kappa^P_{31} = \ldots = \kappa^P_{23} = 0$	67,646.63	33	0.0063	-135,227.3	-135,052.8
(9) $\kappa^P_{31} = \ldots = \kappa^P_{24} = 0$	67,643.30	32	0.0099	-135,222.6	-135,053.4
(10) $\kappa^P_{31} = \ldots = \kappa^P_{13} = 0$	67,636.81	31	0.0003	-135,211.6	-135,047.7

Table 5: **Evaluation of Alternative Specifications of the Regime-Switching Model.** Ten alternative estimated specifications of the regime-switching model are evaluated. Each specification is listed with its maximum log likelihood ($\log L$), number of parameters (k), and the p-value from a likelihood ratio test of the hypothesis that the specification differs from the one directly above that has one more free parameter. The information criteria (AIC and BIC) are also reported, and their minimum values are given in boldface.

4.1 Model Selection and Fit

For estimating the probability of exiting the zero-bound state, as well as for forecasting, the specification of the mean-reversion matrix K^P is critical. To select the best fitting specification of the model's real-world dynamics, I use a general-to-specific modeling strategy that restricts the least significant off-diagonal parameter of K^P to zero and then re-estimates the model. This strategy of eliminating the least significant coefficients is carried out down to the most parsimonious specification, which has a diagonal K^P matrix. The final specification choice is based on the values of the Akaike and Bayes information criteria as per Christensen et al. (2010) (see, e.g., Harvey 1989).[20]

The summary statistics of the model selection process are reported in Table 5. The Akaike information criterion is minimized by specification (5), which has a K^P matrix given by

$$K^P_{AIC} = \begin{pmatrix} \kappa^P_{11} & 0 & \kappa^P_{13} & 0 \\ \kappa^P_{21} & \kappa^P_{22} & \kappa^P_{23} & \kappa^P_{24} \\ 0 & 0 & \kappa^P_{33} & \kappa^P_{34} \\ 0 & 0 & 0 & \kappa^P_{44} \end{pmatrix},$$

[20] The Akaike information criterion is defined as AIC $= -2\log L + 2k$, where k is the number of model parameters, while the Bayes information criterion is defined as BIC $= -2\log L + k\log T$, where T is the number of data observations. The data set contains 1,461 weekly observations for the full sample, but only 211 observations of η_t in the zero-bound state. Still, T is interpreted as referring to the longest data series and is fixed at 1,461.

K^P	$K^P_{\cdot,1}$	$K^P_{\cdot,2}$	$K^P_{\cdot,3}$	$K^P_{\cdot,4}$	θ^P		Σ
$K^P_{1,\cdot}$	0.2400	0	-0.1580	0	0.0637	σ_L	0.0068
	(0.0836)		(0.0433)		(0.0083)		(0.0001)
$K^P_{2,\cdot}$	0.2606	0.3555	-0.4348	0.0392	-0.0245	σ_S	0.0108
	(0.1915)	(0.1381)	(0.1143)	(0.0110)	(0.0102)		(0.0002)
$K^P_{3,\cdot}$	0	0	0.9346	-0.0859	-0.0176	σ_C	0.0273
			(0.2070)	(0.0324)	(0.0055)		(0.0005)
$K^P_{4,\cdot}$	0	0	0	0.5863	1.0104	σ_η	1.0885
				(0.3595)	(0.0917)		(0.0965)

Table 6: **Estimated Parameters in Regime-Switching Model.** The estimated parameters of the K^P matrix, θ^P vector, and diagonal Σ matrix for the regime-switching model are shown. The estimated value of λ is 0.4729 (0.0030), while $\kappa^Q_\eta = 0.3599$ (0.1378) and $\theta^Q_\eta = 2.3707$ (0.7240). The numbers in parentheses are the estimated parameter standard deviations. The maximum log likelihood value is 67,658.84.

while the Bayes information criterion prefers the more parsimonious specification (6) with a K^P matrix given by

$$K^P_{BIC} = \begin{pmatrix} \kappa^P_{11} & 0 & \kappa^P_{13} & 0 \\ 0 & \kappa^P_{22} & \kappa^P_{23} & \kappa^P_{24} \\ 0 & 0 & \kappa^P_{33} & \kappa^P_{34} \\ 0 & 0 & 0 & \kappa^P_{44} \end{pmatrix}.$$

In light of the relatively low number of observations from the zero-bound state, the BIC might impose a penalty for including additional parameters that is too large. For that reason I choose to focus on the specification preferred by AIC in the remainder of the paper.

For the upper 3×3 part of the mean-reversion matrix K^P, that represents the factor dynamics in the normal state, the preferred specification is close to the specification favored by CR, who went through a careful and extensive model selection process to find a well-specified AFNS model of U.S. Treasury yields for the 1987-2010 period.[21] However, they impose a unit-root property on the Nelson-Siegel level factor to improve forecast performance and mitigate issues related to the finite-sample upward bias in the estimated parameters of the K^P mean-reversion matrix.[22] I choose not to do that as it seems to interfere with the estimation of the off-diagonal elements in the fourth column of K^P. Furthermore, due to the long sample and the estimated high persistence of the state variables, there would only be modest gains from correcting for the finite-sample bias in the estimated parameters of K^P, which would not warrant the added computational burden.

Table 6 contains the estimated model parameters. As noted above, the level factor is the most persistent factor. The slope factor is also very persistent with a rate of mean-reversion

[21] The only difference relative to their specification is that they impose the additional restriction that $\kappa^P_{13} = 0$.

[22] See Bauer et al. (2012) for a detailed discussion of this problem in the context of Gaussian dynamic term structure models.

of around 0.35, while the curvature factor is less persistent and more volatile. Finally, the η_t intensity process for the switch out of the zero-bound state is less persistent than the slope factor, but more persistent than the curvature factor.

In the remainder of this subsection, additional estimation results from the regime-switching model are studied in some detail and compared to those obtained from estimating the standard AFNS model that preserves the normal-state dynamics in the preferred specification of the regime-switching model throughout.[23]

Figure 6 shows the factor loadings of the state variables in the zero coupon bond yield function in the zero-bound state and compares them to those in the normal state.[24] First, we note the significant drop in the sensitivity of short-term yields to variation in the level factor, which is more pronounced the lower the value of η_t. Second, the slope factor has a factor loading across maturities very similar to that of a curvature factor, which largely reflects the fact that the slope factor has no role to play for the shortest yield maturities in the zero-bound state. Again, this effect is more pronounced the lower the value of η_t, as an exit to the normal state is less likely. Third, and maybe not surprisingly, the curvature factor preserves a factor loading close to that of the normal state and is not very sensitive to variations in η_t. Finally, Figure 6(d) shows the factor loading of η_t. It exhibits a hump-shaped pattern, which is more pronounced the lower the value of η_t, with a peak near the one- to two-year maturity. When η_t is low, the economy is likely to remain in the zero-bound state for longer. As a consequence, bond yields become more sensitive to news about η_t.

Figure 7 illustrates the estimated paths of the four state variables over the part of the sample that covers the zero-bound period. Note that for the first three factors (level, slope, and curvature), the results are compared to those we get from estimating the normal-state three-factor AFNS model on the full sample without imposing any regime switch. As shown in Figure 7(a), the level factor is little affected by the incorporation of the regime switch. Intuitively, if the economy is expected to return to the normal state in the foreseeable future, there should not be a sizeable wedge in long-term bond yields across the two regimes. Obviously, the slope factor is a different story. In the regime-switching model, this factor is systematically above the path from the standard model as shown in Figure 7(b) since it does not have to match the very low level of the shortest yields in the zero-bound state. To preserve the fit of medium-term yields, the higher path of the slope factor in the regime-switching model is offset by a slightly lower path for the curvature factor than in the standard model as illustrated in Figure 7(c). Despite these differences it should be noted that the time variation

[23] It is worth emphasizing that none of the results discussed in this subsection are sensitive to the specific choice of mean-reversion matrix K^P in either the standard or the regime-switching model.

[24] As the zero coupon bond yield function is nonlinear in the zero-bound state, the shown factor loadings are calculated as first-order approximations with the first three state variables fixed at their full sample averages, while η_t takes on two different values (see the caption of the figure for details).

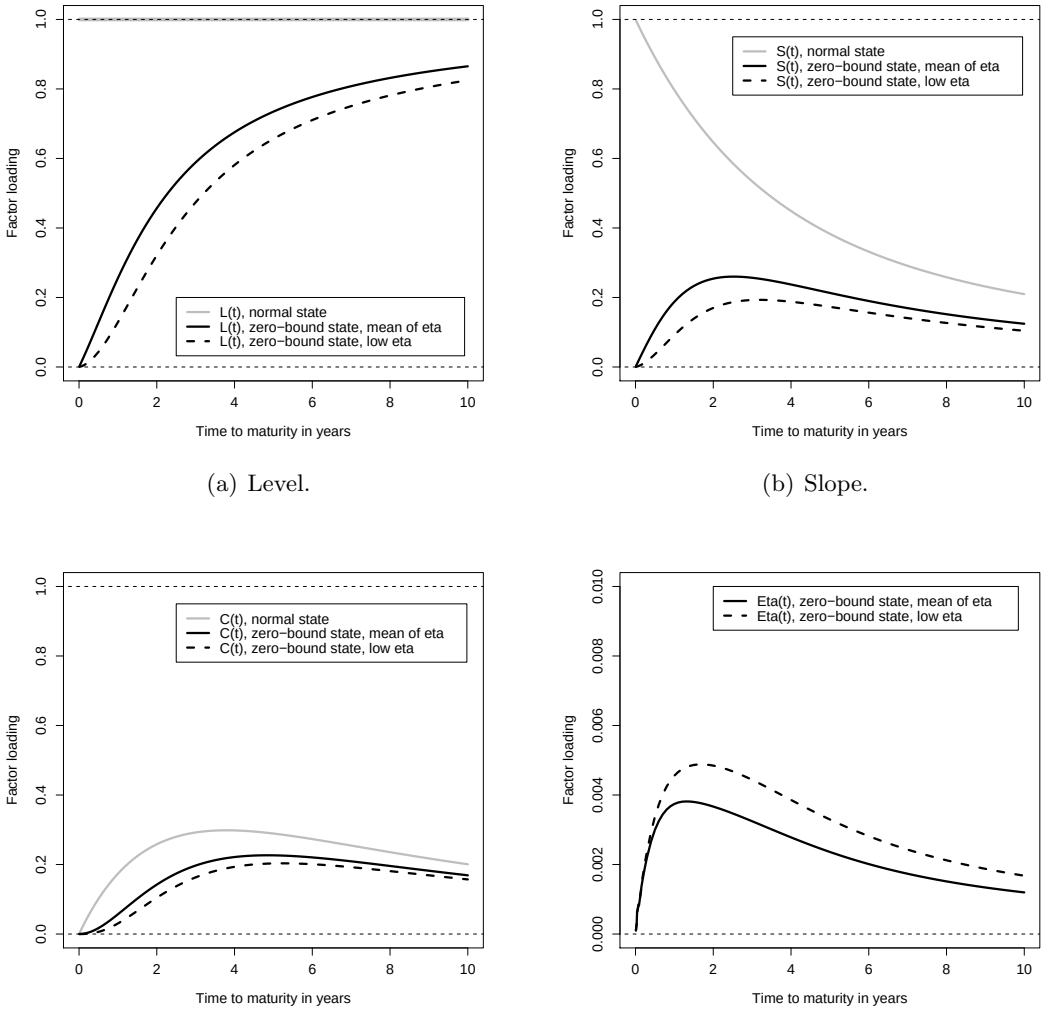

(a) Level.

(b) Slope.

(c) Curvature.

(d) η_t process.

Figure 6: **Factor Loadings in Yield Function.** Illustration of the factor loadings in the zero coupon bond yield function. For the level, slope, and curvature factors both the normal and the zero-bound state loadings are shown. For the zero-bound state, loadings are shown both assuming the estimated average value of η_t as well as a low value of $\eta_t = 0.05$, while the three other state variables are fixed at their full sample averages. The parameters used in the calculations are those estimated on the full sample covering the period from January 4, 1985, to December 28, 2012.

is very highly correlated across the two models for these three factors. Finally, as shown in Figure 7(d), the path of η_t is rather volatile with notable cycles around a general lower trend that is the result of the slow recovery after the financial crisis and the related downward revisions to the outlook for future monetary policy as I will demonstrate later.

Table 7 shows the summary statistics of the fitted errors from the regime-switching model introduced in this paper and those from the standard AFNS model that preserves the normal state dynamics of the regime-switching model throughout. In each case, the summary

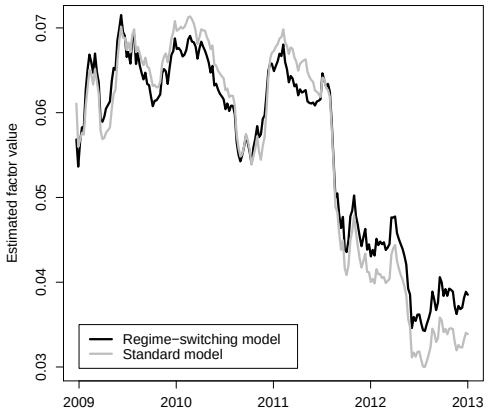

(a) Estimated level factors.

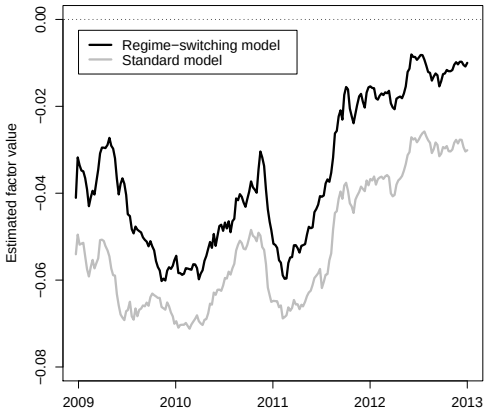

(b) Estimated slope factors.

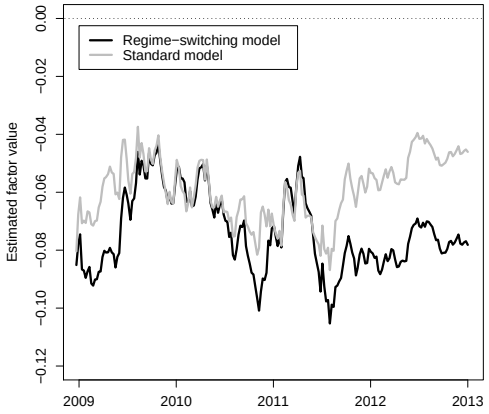

(c) Estimated curvature factors.

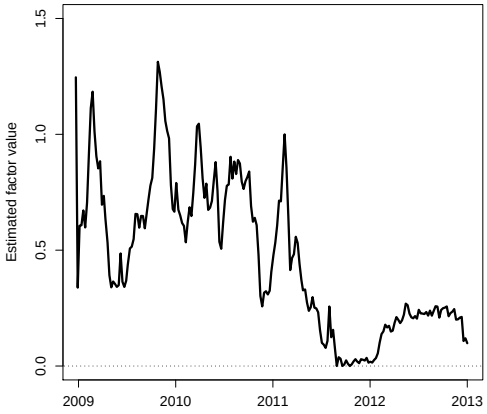

(d) Estimated η_t process.

Figure 7: **Estimated Factor Paths.** Illustration of the estimated factor paths in the regime-switching model. For the level, slope, and curvature factors the results are compared to those of the standard three-factor AFNS model that preserves the normal state dynamics of the preferred regime-switching model specification throughout. The shown period covers the zero-bound state from December 19, 2008, to December 28, 2012, while the full sample used in model estimation covers the period from January 4, 1985, to December 28, 2012.

statistics are calculated for two subsamples. The first is the normal state period that lasted until December 12, 2008, the other is the zero-bound state period from December 19, 2008, through 2012. We note that both models underperform in fitting the short-term yields in the normal state. However, that does not matter much when yields are far from the zero bound. On the contrary, once in the zero-bound state where three- and six-month yields have averaged 10 and 18 basis points, respectively, it is not satisfactory to have RMSEs on the order of 22 and 13 basis points, respectively. Thus, as expected, the introduction of the

Maturity in months	Normal state			
	Standard model		Regime-switching model	
	Mean	RMSE	Mean	RMSE
3	-16.78	32.71	-17.23	32.95
6	-5.93	15.64	-6.17	15.72
12	0.00	0.00	0.00	0.00
24	1.39	2.51	1.48	2.49
36	0.00	0.00	0.00	0.00
60	-1.83	3.01	-1.97	2.92
84	0.25	2.57	0.23	2.07
120	7.73	10.56	8.24	10.57
Maturity in months	Zero-bound state			
	Standard model		Regime-switching model	
	Mean	RMSE	Mean	RMSE
3	-17.34	22.37	0.79	3.92
6	-9.78	12.51	-0.11	2.47
12	0.00	0.00	0.80	2.02
24	0.93	1.73	-0.92	2.19
36	0.00	0.00	0.37	1.81
60	-1.33	3.10	0.15	0.69
84	0.10	3.67	-0.17	1.55
120	4.53	10.82	0.09	3.80

Table 7: **Summary Statistics of Fitted Errors.** The mean fitted errors and the root mean squared fitted errors (RMSE) from the four-factor regime-switching model of U.S. Treasury yields as well as those from the standard three-factor AFNS model that preserves the normal state dynamics of the regime-switching model throughout are shown. In each case, the summary statistics are calculated for two periods: (1) the normal state period from January 4, 1985, to December 12, 2008, and (2) the zero-bound state period from December 19, 2008, to December 28, 2012. The full sample used in each model estimation is weekly covering the period from January 4, 1985, to December 28, 2012. All numbers are measured in basis points.

fourth factor with its unique characteristics is beneficial for the fit of the short-term yields. To understand the difference in the results across the two models, Figure 8 shows the fitted yield curves from both models as well as the observed yields at the end of the sample. The failure of the standard model in fitting short-term yields near the zero lower bound is evident, as is the equally clear success of the regime-switching model to do just that.

4.2 Yield Volatility in the Zero-Bound State

In this section, I document that the regime-switching model produces notably lower short-term yield volatility in the zero-bound state as compared to the normal state.

To provide evidence of the model's ability to match yield volatility near the zero lower bound, I compare the model's conditional one-month projection of yield volatility at various maturities to a measure of the subsequent 31-day realized yield volatilities.

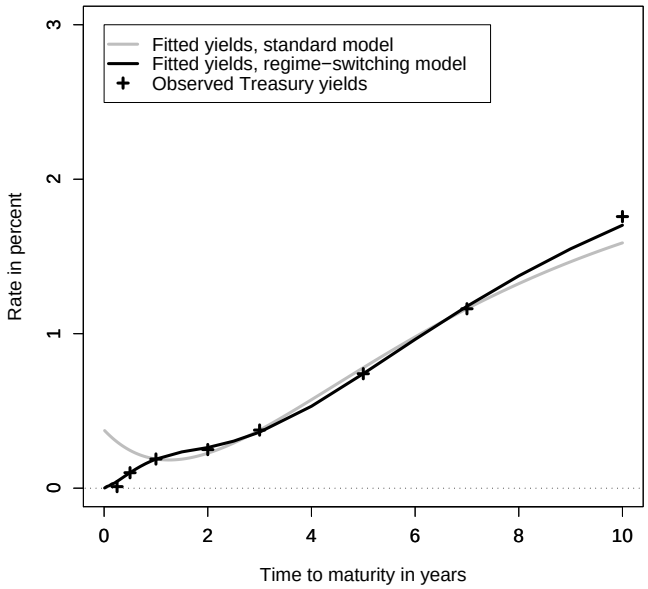

Figure 8: **Fitted Yield Curves.** Illustration of the fitted yield curve as of December 28, 2012, from the four-factor regime-switching model of U.S. Treasury yields as well as that from the standard three-factor AFNS model that preserves the normal state dynamics of the regime-switching model throughout.

In the normal state, where zero coupon yields are affine functions of the state variables, model-implied conditional predicted yield volatilities are given by the square root of

$$V_t^P[y^N(T,T+\tau)] = \frac{1}{\tau^2} B^N(T,T+\tau)' V_t^P[X_T] B^N(T,T+\tau), \tag{6}$$

where $T-t$ is the prediction period, τ is the yield maturity, and $V_t^P[X_T]$ is the conditional covariance matrix, which for affine diffusion processes in general is given by[25]

$$V^P[X_T|X_t] = \int_t^T \exp(-K^P(T-s))\Sigma D(E^P[X_s|X_t]) D(E^P[X_s|X_t])'\Sigma' \exp(-(K^P)'(T-s))ds. \tag{7}$$

In the zero-bound state, where zero coupon yields are nonlinear functions of the state variables, model-implied conditional predicted yield volatilities must be generated by simulation.

In the following, I focus on the one-month conditional yield volatilities generated by the regime-switching model during the zero-bound state since 2009.

To evaluate the fit of these predicted one-month-ahead conditional yield standard devi-

[25] The conditional covariance matrix is calculated using the analytical solutions provided in Fisher and Gilles (1996).

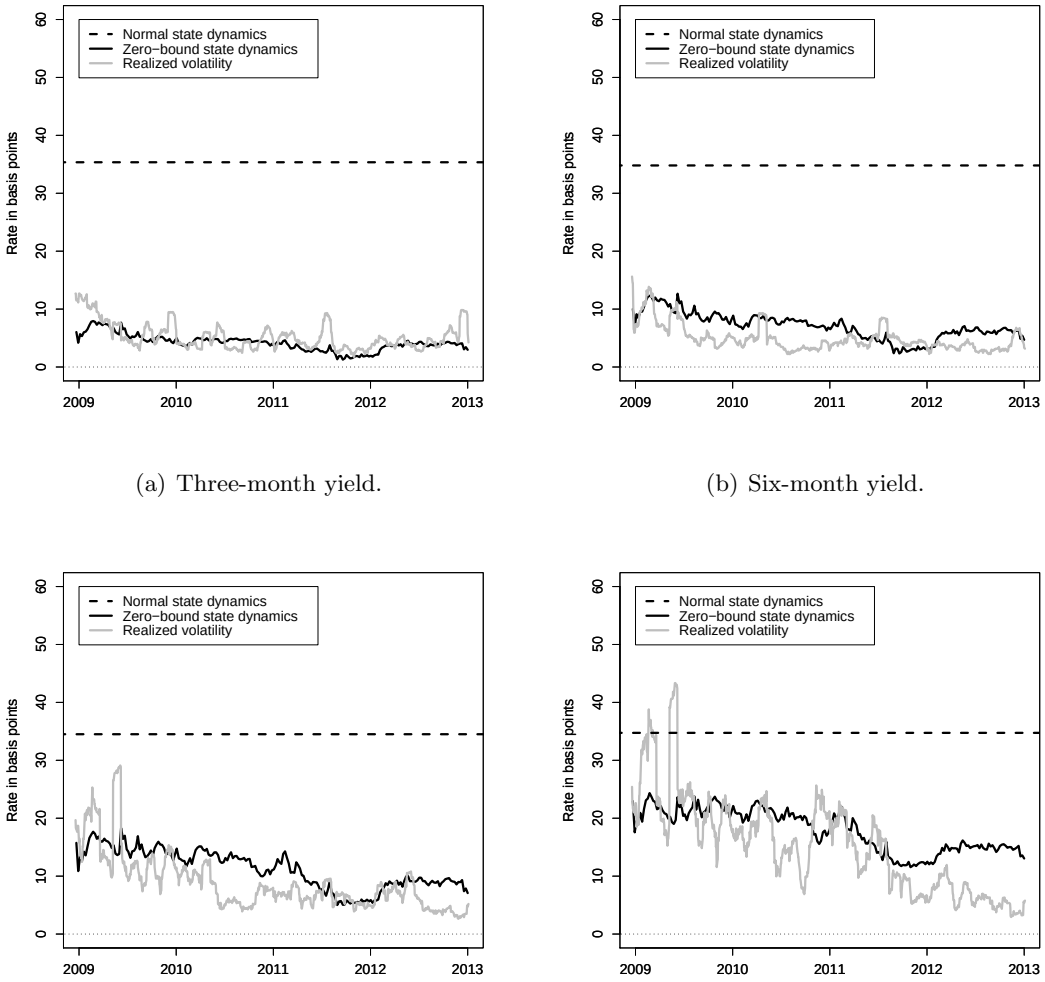

(a) Three-month yield.

(b) Six-month yield.

(c) One-year yield.

(d) Two-year yield.

Figure 9: **One-Month Conditional Yield Volatilities.** Illustration of the one-month conditional volatility of the three-month, six-month, one-year, and two-year Treasury yields implied by the estimated regime-switching model using both its normal state and zero-bound state P-dynamics. Also shown are the subsequent 31-day realized volatility series calculated based on daily data as described in the main text. The period shown covers the zero-bound state from December 19, 2008, to December 28, 2012, while the full sample used in model estimation covers the period from January 4, 1985, to December 28, 2012.

ations, I compare them to a standard measure of realized volatility based on the same data used in the model estimation, but at daily frequency. The realized standard deviation of the daily changes in the interest rates are generated for the 31-day period ahead on a rolling basis. The realized variance measure is used by Andersen and Benzoni (2010), Collin-Dufresne et al. (2009), and Jacobs and Karoui (2009) in their assessments of stochastic volatility models. This measure is fully nonparametric and has been shown to converge to the underlying realization of the conditional variance as the sampling frequency increases; see Andersen et

al. (2003) for details. The square root of this measure retains these properties. For each observation date t the number of trading days N during the subsequent 31-day time window is determined (where N is most often 21 or 22) and the realized standard deviation is calculated as

$$RV_{t,\tau}^{STD} = \sqrt{\sum_{n=1}^{N} \Delta y_{t+n}^2(\tau)},$$

where $\Delta y_{t+n}(\tau)$ is the change in yield $y(\tau)$ from trading day $t+(n-1)$ to trading day $t+n$.[26]

Figure 9 shows the results for four yield maturities: three-month, six-month, one-year, and two-year. In the normal state, the yields with two years or less to maturity have near identical conditional one-month yield volatilities of about 35 basis points, which are all constant due to the Gaussian dynamics. In the zero-bound state, the regime-switching model produces projected yield volatilities for short-term yields that closely match the corresponding subsequent yield volatility realizations. However, further out the yield curve the model starts to approximate the normal state dynamics characterized by constant yield volatility. Still, the model continues to provide a fairly close fit to those realized yield volatility series. Furthermore, as can be seen in Figure 9(d), there remains a clear wedge between the normal state and zero-bound state yield volatility dynamics, even at the longer maturities.[27]

4.3 Exit from the Zero-Bound State

In this section, I analyze the model-implied distribution of the exit time from the zero-bound state.

The estimated probability of remaining in the zero-bound state is given by

$$E_t^P\left[e^{-\int_t^T \eta_u du}\right] = \exp\left(A_\eta^P(t,T) + B_\eta^P(t,T)\eta_t\right), \tag{8}$$

while the continuous intensity of exiting the zero-bound state is

$$E_t^P\left[\eta_T e^{-\int_t^T \eta_u du}\right] = \exp\left(A_\eta^P(t,T) + B_\eta^P(t,T)\eta_t\right) \times \left[C_\eta^P(t,T) + D_\eta^P(t,T)\eta_t\right], \tag{9}$$

[26] Note that other measures of realized volatility have been used in the literature, such as the realized mean absolute deviation measure as well as fitted GARCH estimates. Collin-Dufresne et al. (2009) also use option-implied volatility as a measure of realized volatility.

[27] Unreported results show that the fit of long-term yield volatilities can be improved through the incorporation of stochastic volatility into the Nelson-Siegel level factor as in Christensen et al. (2012). However, this is left for future refinement.

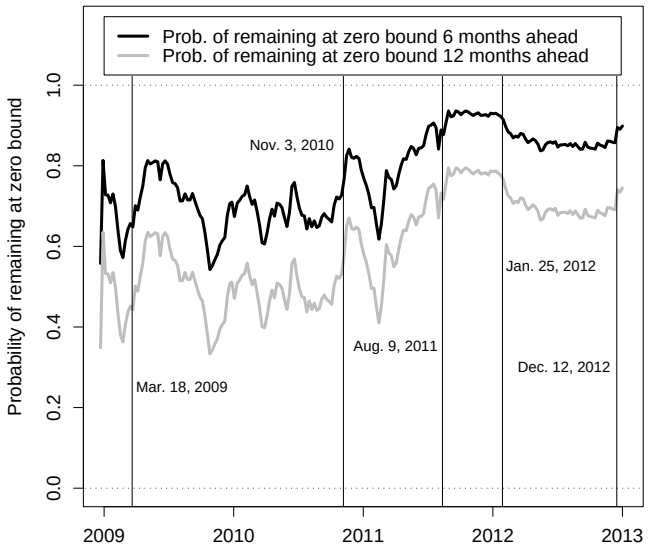

Figure 10: **Probability of Remaining in the Zero-Bound State.** Illustration of the estimated probability of remaining in the zero-bound state six and twelve months ahead. The sample used in model estimation consists of weekly U.S. Treasury zero-coupon bond yields covering the period from January 4, 1985, to December 28, 2012.

where[28]

$$
\begin{aligned}
A_\eta^P(t,T) &= \frac{2\kappa_{44}^P\theta_4^P}{\sigma_\eta^2}\ln\left[\frac{2\phi_\eta^P e^{\frac{1}{2}(\phi_\eta^P+\kappa_{44}^P)(T-t)}}{2\phi_\eta^P+(\phi_\eta^P+\kappa_{44}^P)(e^{\phi_\eta^P(T-t)}-1)}\right],\\
B_\eta^P(t,T) &= \frac{-2(e^{\phi_\eta^P(T-t)}-1)}{2\phi_\eta^P+(\phi_\eta^P+\kappa_{44}^P)[e^{\phi_\eta^P(T-t)}-1]},\\
C_\eta^P(t,T) &= 2\kappa_{44}^P\theta_4^P\frac{e^{\phi_\eta^P(T-t)}-1}{2\phi_\eta^P+(\phi_\eta^P+\kappa_{44}^P)(e^{\phi_\eta^P(T-t)}-1)},\\
D_\eta^P(t,T) &= \frac{4(\phi_\eta^P)^2e^{\phi_\eta^P(T-t)}}{\left[2\phi_\eta^P+(\phi_\eta^P+\kappa_{44}^P)(e^{\phi_\eta^P(T-t)}-1)\right]^2}
\end{aligned}
$$

with

$$\phi_\eta^P=\sqrt{(\kappa_{44}^P)^2+2\sigma_\eta^2}.$$

The estimated probability of remaining in the zero-bound state is illustrated in Figure 10 at the six- and twelve-month forecast horizon. The lower trending path for the η_t process

[28] These results are obtained by combining the P-dynamics of the η_t-process with analytical formulas provided in Christensen (2007).

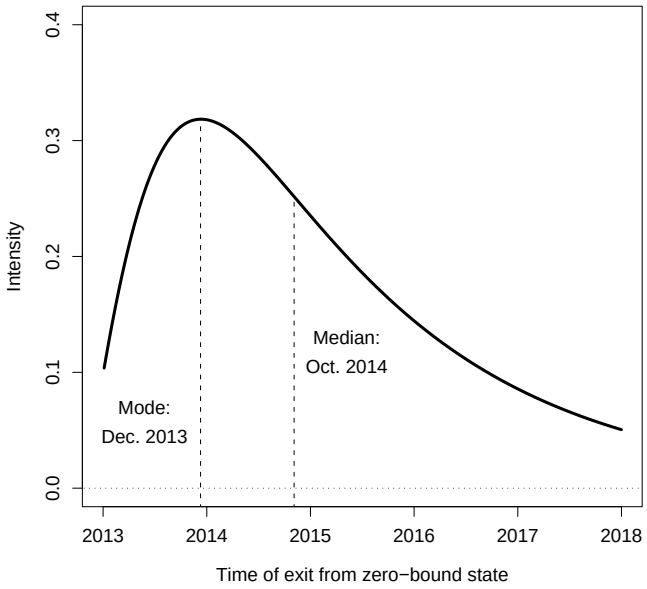

Figure 11: **Distribution of the Exit Time from the Zero-Bound State.** The figure illustrates the continuous intensity of exiting the zero-bound state as of December 28, 2012. Vertical dashed lines indicate both the mode and the median of the exit time distribution.

converts into an upward trending path for the probability of remaining in the zero-bound state. Also, included are five key dates with major decisions by the FOMC regarding either its LSAP programs or its forward guidance for future policy. In the weeks after each announcement there are notable upward spikes in the estimated probability of remaining at the zero bound. The extension of the forward guidance at the January 2012 FOMC meeting is the notable exception. This suggests that part of the effect from unconventional policies comes from a signaling channel through which the FOMC policy actions are interpreted to indicate that the policy rate will remain at its lower bound longer, as also emphasized by Bauer and Rudebusch (2013b) and CR.

Figure 11 shows the continuous intensity of exiting the zero-bound state as of December 28, 2012. The mode is attained in late 2013, notably earlier than the forward guidance provided by the FOMC at the time, which indicated that zero interest rates were likely until at least mid-2015. However, the distribution is heavily skewed to the right so the mode is not the appropriate statistic to focus on in order to describe the exit time distribution, even though it obviously indicates the most likely exit date. Instead, I focus on the median exit time, that is, the exit time that splits the probability mass in half, which is also indicated with a vertical dashed line. It is located in October 2014, relatively close to the forward guidance provided in FOMC statements. The variation in the estimated median exit time from the

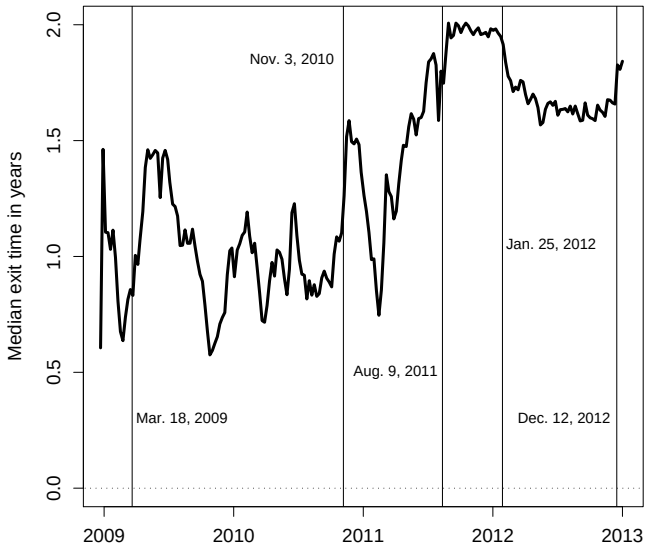

Figure 12: **Median Exit Time from the Zero-Bound State.** Illustration of the estimated median exit time from the zero-bound state from December 19, 2008, to December 28, 2012.

zero-bound state since December 19, 2008, is shown in Figure 12. As in Figure 10, four of the five key FOMC announcements had significant positive effects on the median exit time. Furthermore, it is not far from its all-time high at the end of the sample.

5 Monetary Policy Expectations and Term Premiums

Here, I first describe how future short rate expectations are calculated within the regime-switching model and analyze how they have varied in recent years. I also discuss the model's decomposition of long-term yields into policy expectations and term premium components. Finally, I analyze the model's yield projections.

5.1 Monetary Policy Expectations in the Zero-Bound State

The objective of this section is to assess the reasonableness of the derived monetary policy expectations from the regime-switching model by comparing them to those derived from a standard term structure model and to those implied by the rates on federal funds futures contracts.

In the zero-bound state, the expected short rate τ years ahead is given by[29]

$$\begin{aligned} E_t^P[r_{t+\tau}] &= 0 \cdot E_t^P\Big[e^{-\int_t^{t+\tau}\eta_u du}\Big] + E_t^P\Big[\int_t^{t+\tau}\eta_s e^{-\int_t^s \eta_u du} r_{t+\tau} ds\Big] \\ &= \int_t^{t+\tau} E_t^P\Big[\eta_s e^{-\int_t^s \eta_u du} E_s^P[r_{t+\tau}]\Big] ds. \end{aligned}$$

Ideally, the regime-switching model's accuracy in projecting future short rates should be tested in a real-time forecast exercise over many years like the one performed by CR. However, the limited data from the zero-bound state prevents such an exercise at the time of this writing. Instead, to assess the regime-switching model's short-rate projections during the most recent period, I use the full-sample estimation results and compare the variation in the one- and two-year short rate forecasts from the regime-switching model to the corresponding results from the standard AFNS model favored by CR, referred to as the CR model, and to the rates on one- and two-year federal funds futures contracts, all shown in Figure 13.[30] In doing so, it should be emphasized that the existence of time-varying risk premiums even in very short-term federal funds futures contracts is well documented (see Piazzesi and Swanson 2008). However, the risk premiums in such short-term contracts are small relative to the sizeable variation observed during the time period shown in Figure 13. As a consequence, I interpret the bulk of the variation from 2007 to 2009 as reflecting declines in short rate expectations. Furthermore, since August 2011, most evidence—including the one shown in Figure 14 below—suggests that risk premiums have been significantly depressed, likely to a point that the zero-risk-premium assumption for the futures contracts applied here may provide a satisfactory approximation. Combined, these observations suggest that it is defensible for most of the shown six-year period to map the models' short rate projections to the rates on the federal funds futures contracts *without* adjusting them for risk premiums.

At the one-year and two-year forecast horizons, the correlations between the CR model short rate forecasts and the federal funds futures rates are 0.96 and 0.85, respectively. The corresponding correlations for the regime-switching model are 0.96 and 0.87, respectively. For the CR model, the distance to the futures rates measured by the root mean squared errors (RMSE) are 43.26 and 82.24 basis points at the one- and two-year horizon, respectively, while for the regime-switching model the corresponding RMSEs are 50.87 and 89.04 basis points, respectively. Thus, both measured by correlations and by a distance metric, the regime-switching model's short rate projections are about as closely aligned with the information

[29] Appendix B describes the calculation of these expectations.

[30] The futures data are from Bloomberg. The one-year futures rate is the weighted average of the rates on the 12- and 13-month federal funds futures contracts, while the two-year futures rate is the rate on the 24-month federal funds futures contract through 2010, and the weighted average of the rates on the 24- and 25-month contracts since then. Absence of data on the 24-month contracts prior to 2007 determines the start date for the analysis.

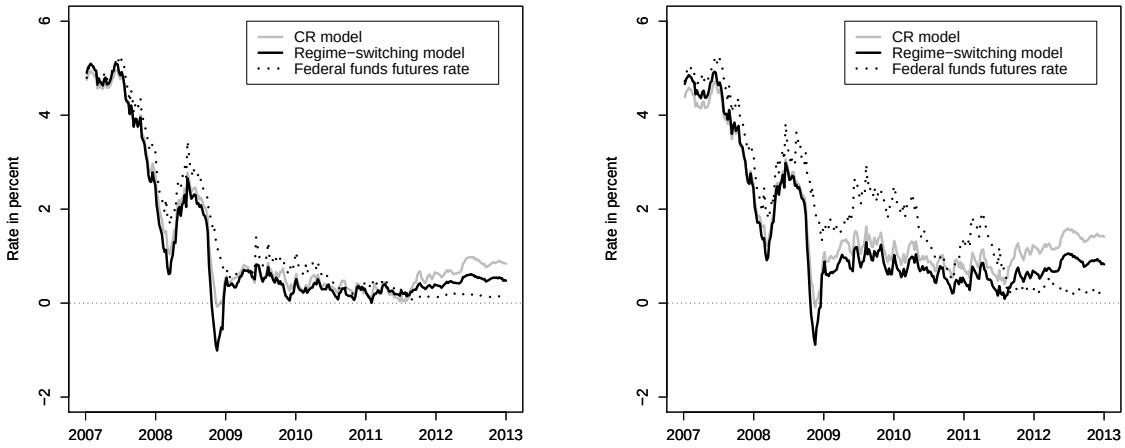

(a) One-year projections.

(b) Two-year projections.

Figure 13: **Comparison of Short Rate Projections.**
Panel (a) illustrates the one-year short rate projections from the CR and regime-switching models with a comparison to the rates on one-year federal funds futures. Panel (b) shows the corresponding results for a two-year projection period with a comparison to the rates on two-year federal funds futures. The data are weekly covering the period from January 5, 2007, to December 28, 2012.

reflected in rates on federal funds futures as the projections generated by the standard CR model for the entire six-year period. Still, it is visually clear from Figure 13 that the short rate expectations from the regime-switching model are closer to the futures rates since August 2011.

5.2 Term Premium Decomposition

In general, the term premium component in the yield of a zero-coupon bond with maturity in τ years is defined as

$$TP_t(\tau) = y(t, t+\tau) - \frac{1}{\tau}\int_t^{t+\tau} E_t^P[r_s]ds$$

and reflects the difference between the long-term yield that can be settled today and the expected return from a rollover strategy that earns the risk-free rate.

In the normal state, the term premium takes its usual form

$$TP_t^N(\tau) = y^N(t, t+\tau) - \frac{1}{\tau}\int_t^{t+\tau} E_t^P[r_s]ds,$$

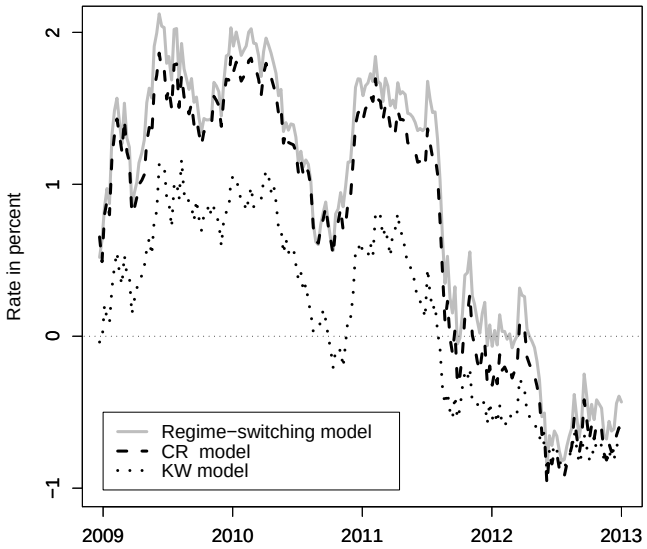

Figure 14: **Estimated Ten-Year Term Premiums.** Illustration of the estimated ten-year zero-coupon term premium from the regime-switching model with a comparison to the corresponding estimates from the CR and KW models. The data shown cover the period from December 19, 2008, to December 28, 2012.

where the instantaneous short rate is the sum of the first two factors

$$r_t = L_t + S_t.$$

In the zero-bound state, the formula for the term premium is given by

$$\begin{aligned} TP_t^Z(\tau) &= y^Z(t, t+\tau) - \frac{1}{\tau}\Big(0 \cdot E_t^P[e^{-\int_t^{t+\tau} \eta_u du}] + E_t^P[\int_t^{t+\tau} \eta_s e^{-\int_t^s \eta_u du} \int_s^{t+\tau} r_u du ds]\Big) \\ &= y^Z(t, t+\tau) - \frac{1}{\tau}\int_t^{t+\tau} E_t^P\Big[\eta_s e^{-\int_t^s \eta_u du} E_s^P[\int_s^{t+\tau} r_u du]\Big] ds. \end{aligned}$$

Appendix C shows how term premiums are calculated in both the normal state and the zero-bound state. The results for the ten-year term premium since 2009 are illustrated in Figure 14. For comparison, the figure also includes the term premium estimates from the CR model and from another established U.S. Treasury yield curve model, the KW model maintained at the Federal Reserve Board. The term premiums are negative and close to all-time lows at the end of the sample, which suggests that, at that point, it could be difficult to provide additional monetary stimulus without materially changing investors' expectations for future monetary policy. Furthermore, we note that the term premium estimates from the

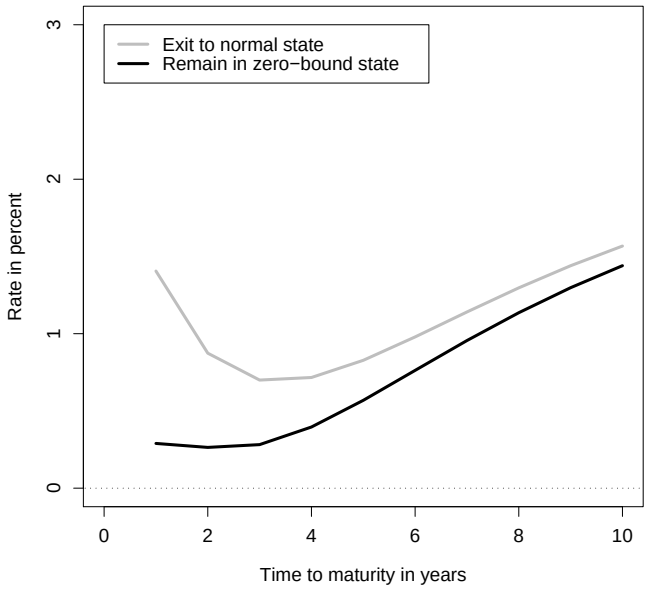

Figure 15: **Forecasted Yield Curves One Year Ahead.** Illustration of the forecasted yield curves one year ahead as of December 28, 2012, contingent on whether the economy remains in the zero-bound state or exits to the normal state.

regime-switching model track those from the CR model very closely since 2009. However, its estimated term premiums are slightly larger, on average, and a little more volatile.

5.3 Yield Curve Projections

As a final exercise, I use the regime-switching model to forecast the yield curve one year ahead as of the end of the sample depending on whether the economy remains in the zero-bound state or manages to exit to the normal state before the end of the forecast horizon.

Figure 15 illustrates the result of this exercise. Contingent on the economy exiting to the normal state over the forecast horizon, the one- and two-year yields would be 112 and 61 basis points higher than otherwise, respectively, while the wedge between the outcome-contingent forecasts of long-term yields is much smaller as investors expect the economy to exit at some point before the maturity of those bonds. This type of forecast exercise could be useful for risk management purposes. Alternatively, it could be used to stress test banks' portfolios as part of assessing their capital adequacy while in the zero-bound state.

6 Conclusion

In this paper, I extend the existing literature on regime-switching models of the yield curve by modifying a standard three-factor term structure model to account for the special dynamics of the Treasury yield curve when the monetary policy instrument is at its effective zero bound. Specifically, I introduce an additional regime referred to as the zero-bound state in which the instantaneous risk-free rate is constant at zero. The novel feature of the model is that the probability of returning to the normal state is allowed to be time-varying under both the objective and the risk-neutral probability measures.

The highlight of the model is that it delivers estimates of the time-varying probability of the economy leaving the zero-bound state within any relevant forecast horizon. Also, the model provides outcome-contingent forecasts of future yield curves depending on whether the economy remains in the zero-bound state or exits to the normal state during the forecast period. This could be useful for stress tests of bond portfolios and for portfolio risk management in general while in the zero-bound state. Finally, the model is arbitrage-free, tractable, delivers a good fit, and matches the compression of yield volatility since 2009.

The results show that during the 2009-2012 period the exit probabilities generally declined, consistent with the efforts by the FOMC to provide more monetary stimulus to support the tepid recovery. Furthermore, the yield curve projections at the end of the sample suggest that, in the less likely event of an exit to the normal state over the following year, one- and two-year yields would be 112 and 61 basis points higher than otherwise, respectively, while the ten-year yield would show much more modest increases as markets have already priced a high probability that the U.S. economy will return to the normal state before its maturity, making the specific timing of the regime switch less relevant for such long-term yields.

It is prudent to note that the model does not impose a zero lower boundary for the model-implied bond yields. However, this could be obtained by incorporating stochastic volatility into the three state variables in the normal state along the lines of Christensen et al. (2013). Such refinements are left for future research.

Appendix A: Kalman Filter Estimation of the Regime-Switching Model

The estimation of the regime-switching model is based on the Kalman filter, but is nonstandard for two reasons. First, we need to handle the switch to the zero-bound state in mid-December 2008. Second, once the economy is in the zero-bound state, zero-coupon bond yields are no longer affine functions of the state variables and the fourth state variable has non-Gaussian dynamics. For a start, though, it is important to note that, in the normal state, the model is Gaussian and identical to the AFNS models introduced in CDR. Hence, for that part of the sample, the Kalman filter algorithm proceeds as described in CDR and repeated here for convenience in order to detail the adjustments needed to do filtering in the zero-bound state.

For the affine Gaussian models, in general, the conditional mean vector and the conditional covariance matrix are

$$\begin{aligned} E^P[X_T|\mathcal{F}_t] &= (I - \exp(-K^P\Delta t))\theta^P + \exp(-K^P\Delta t)X_t, \\ V^P[X_T|\mathcal{F}_t] &= \int_0^{\Delta t} e^{-K^P s}\Sigma\Sigma' e^{-(K^P)'s} ds, \end{aligned}$$

where $\Delta t = T - t$. We compute conditional moments of discrete observations and obtain the state transition equation

$$X_t = (I - \exp(-K^P\Delta t))\theta^P + \exp(-K^P\Delta t)X_{t-1} + \xi_t,$$

where Δt is the time between observations. The measurement equation is (see equation (1))

$$y_t = A + BX_t + \varepsilon_t.$$

The assumed error structure is

$$\begin{pmatrix} \xi_t \\ \varepsilon_t \end{pmatrix} \sim N\left[\begin{pmatrix} 0 \\ 0 \end{pmatrix}, \begin{pmatrix} Q & 0 \\ 0 & H \end{pmatrix}\right],$$

where the matrix H is assumed diagonal, while the matrix Q has the following structure[31]

$$Q = \int_0^{\Delta t} e^{-K^P s}\Sigma\Sigma' e^{-(K^P)'s} ds.$$

In addition, the transition and measurement errors are assumed orthogonal to the initial state.

Now consider Kalman filtering, which is used to evaluate the likelihood function.

Due to the assumed stationarity, the filter is initialized at the unconditional mean and variance of the state variables under the P-measure: $X_0 = \theta^P$ and $\Sigma_0 = \int_0^\infty e^{-K^P s}\Sigma\Sigma' e^{-(K^P)'s} ds$.

Denote the information available at time t by $Y_t = (y_1, y_2, \ldots, y_t)$, and denote model parameters by ψ. Consider period $t-1$ and suppose that the state update X_{t-1} and its mean square error matrix Σ_{t-1} have been obtained. The prediction step is

$$X_{t|t-1} = E^P[X_t|Y_{t-1}] = \Phi_t^{X,0}(\psi) + \Phi_t^{X,1}(\psi)X_{t-1},$$

$$\Sigma_{t|t-1} = \Phi_t^{X,1}(\psi)\Sigma_{t-1}\Phi_t^{X,1}(\psi)' + Q_t(\psi),$$

where $\Phi_t^{X,0} = (I - \exp(-K^P\Delta t))\theta^P$, $\Phi_t^{X,1} = \exp(-K^P\Delta t)$, and $Q_t = \int_0^{\Delta t} e^{-K^P s}\Sigma\Sigma' e^{-(K^P)'s} ds$, while Δt is the time between observations.

[31] Throughout, conditional and unconditional covariance matrices are calculated using the analytical solutions provided in Fisher and Gilles (1996).

In the time-t update step, $X_{t|t-1}$ is improved by using the additional information contained in Y_t:

$$X_t = E[X_t|Y_t] = X_{t|t-1} + \Sigma_{t|t-1}B(\psi)'F_t^{-1}v_t,$$

$$\Sigma_t = \Sigma_{t|t-1} - \Sigma_{t|t-1}B(\psi)'F_t^{-1}B(\psi)\Sigma_{t|t-1},$$

where

$$v_t = y_t - E[y_t|Y_{t-1}] = y_t - A(\psi) - B(\psi)X_{t|t-1},$$
$$F_t = cov(v_t) = B(\psi)\Sigma_{t|t-1}B(\psi)' + H(\psi),$$
$$H(\psi) = diag(\sigma_\varepsilon^2(\tau_1), \ldots, \sigma_\varepsilon^2(\tau_N)).$$

At this point, the Kalman filter has delivered all ingredients needed to evaluate the Gaussian log likelihood, the prediction-error decomposition of which is

$$\log l(y_1, \ldots, y_T; \psi) = \sum_{t=1}^{T} \Big(-\frac{N}{2}\log(2\pi) - \frac{1}{2}\log|F_t| - \frac{1}{2}v_t'F_t^{-1}v_t \Big),$$

where N is the number of observed yields. Now, the likelihood is numerically maximized with respect to ψ using the Nelder-Mead simplex algorithm. Upon convergence, the standard errors are obtained from the estimated covariance matrix,

$$\widehat{\Omega}(\widehat{\psi}) = \frac{1}{T}\Big[\frac{1}{T}\sum_{t=1}^{T}\frac{\partial \log l_t(\widehat{\psi})}{\partial \psi}\frac{\partial \log l_t(\widehat{\psi})}{\partial \psi}'\Big]^{-1},$$

where $\widehat{\psi}$ denotes the estimated model parameters.

The introduction of stochastic volatility in the zero-bound state implies that the factors are no longer simply Gaussian for that part of the sample. The way to proceed is to simply approximate the true probability distribution of the state variables with the first and second moments and use the Kalman filter algorithm *as if* the state variables were Gaussian.[32] Thus, the state equation continues to be given by

$$X_t = (I - \exp(-K^P\Delta t))\theta^P + \exp(-K^P\Delta t)X_{t-1} + \xi_t, \quad \xi_t \sim N(0, V_{t-1}),$$

while the conditional covariance matrix for affine diffusion processes with stochastic volatility is given by

$$V^P[X_T|X_t] = \int_t^T \exp(-K^P(T-s))\Sigma D(E^P[X_s|X_t])D(E^P[X_s|X_t])'\Sigma' \exp(-(K^P)'(T-s))ds.$$

In handling the switch date to the zero-bound state, the approach of Christensen et al. (2010) is followed. For the first 24 years of the sample when the economy is in the normal state, $e^{-K^P\Delta t}$, $(1 - e^{-K^P\Delta t})\theta^P$, and the conditional covariance matrix

$$V^P[X_T|\mathcal{F}_t] = \int_0^{\Delta t} e^{-K^P s}\Sigma\Sigma' e^{-(K^P)'s}ds$$

are calculated using the upper 3×3 part of K^P and the upper 3×1 part of θ^P. Once the economy hits the zero bound on December 16, 2008, the θ^P, K^P and Σ used in the Kalman filter algorithm represent the full

[32] A few notable examples of papers that follow this approach include Duffee (1999), Driessen (2005), and Feldhütter and Lando (2008).

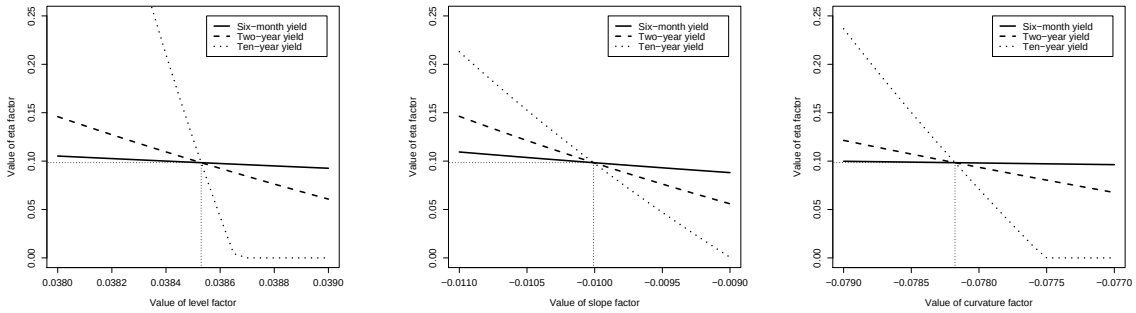

(a) (L_t, η_t) combinations. (b) (S_t, η_t) combinations. (c) (C_t, η_t) combinations.

Figure 16: **Linearity of Yield Function in the Zero-Bound State.** Illustration of the combinations of (L_t, η_t), (S_t, η_t), and (C_t, η_t) that deliver a perfect fit to the six-month, two-year, and ten-year Treasury yields implied by the regime-switching model as of December 28, 2012.

four-dimensional dynamics of the state variables and the conditional covariance matrix is calculated as[33]

$$\int_t^{t+\tau} e^{-K^P(t+\tau-s)}\Sigma D(E^P[X_s|X_t])D(E^P[X_s|X_t])'\Sigma' e^{-(K^P)'(t+\tau-s)}ds.$$

Furthermore, in the zero-bound state, we need to use the extended Kalman filter because the zero-coupon bond yields are no longer affine functions of the state variables. Instead, the measurement equation takes the general form

$$y_t^Z = z(X_t;\psi) + \varepsilon_t^Z.$$

In the extended Kalman filter, this equation is linearized using a first-order Taylor expansion around the best guess of X_t in the prediction step of the Kalman filter algorithm. Thus, in the notation introduced above, this best guess is denoted $X_{t|t-1}$ and the approximation is given by

$$z(X_t;\psi) \approx z(X_{t|t-1};\psi) + \frac{\partial z(X_t;\psi)}{\partial X_t}\Big|_{X_t=X_{t|t-1}}(X_t - X_{t|t-1}).$$

Thus, by defining

$$A_t(\psi) \equiv z(X_{t|t-1};\psi) - \frac{\partial z(X_t;\psi)}{\partial X_t}\Big|_{X_t=X_{t|t-1}} X_{t|t-1}, B_t(\psi) \equiv \frac{\partial z(X_t;\psi)}{\partial X_t}\Big|_{X_t=X_{t|t-1}},$$

the measurement equation can be given on an affine form as

$$y_t^Z = A_t(\psi) + B_t(\psi)X_t + \varepsilon_t^Z$$

and the steps in the algorithm proceed as previously described.

Figure 16 demonstrates that the bond yield function in the zero-bound state is close to linear locally even in the η_t-dimension. This suggests that the approximation error of the extended Kalman filter is likely to be minuscule.

Finally, in the empirical implementation, the measurement error distribution is assumed to switch as well. Hence, both an H^N and H^Z matrix, each with eight $\sigma_\varepsilon^2(\tau_i)$ parameters, are estimated to account for the difference in the size of the fitted errors across the two regimes.

[33] Once the economy exits the zero-bound state, the change in the transition equation is simply reversed.

Appendix B: Policy Expectations in the Regime-Switching Model

In the normal state, the instantaneous rate is the sum of the first two factors

$$r_t = L_t + S_t.$$

In the specification of the regime-switching model preferred according to the AIC, the P-dynamics in the normal state are given by

$$\begin{pmatrix} dL_t \\ dS_t \\ dC_t \end{pmatrix} = \begin{pmatrix} \kappa_{11}^P & 0 & \kappa_{13}^P \\ \kappa_{21}^P & \kappa_{22}^P & \kappa_{23}^P \\ 0 & 0 & \kappa_{33}^P \end{pmatrix} \left[\begin{pmatrix} \theta_1^P \\ \theta_2^P \\ \theta_3^P \end{pmatrix} - \begin{pmatrix} L_t \\ S_t \\ C_t \end{pmatrix} \right] dt + \begin{pmatrix} \sigma_L & 0 & 0 \\ 0 & \sigma_S & 0 \\ 0 & 0 & \sigma_C \end{pmatrix} \begin{pmatrix} dW_t^{L,P} \\ dW_t^{S,P} \\ dW_t^{C,P} \end{pmatrix}.$$

As a consequence, the conditional mean of L_t and S_t in the normal state are given by[34]

$$\begin{aligned}
E_t^P[L_T] &= \theta_1^P + (L_t - \theta_1^P)e^{-\kappa_{11}^P(T-t)} - \kappa_{13}^P(C_t - \theta_3^P)\frac{e^{-\kappa_{33}^P(T-t)} - e^{-\kappa_{11}^P(T-t)}}{\kappa_{11}^P - \kappa_{33}^P}, \\
E_t^P[S_T] &= \theta_2^P + (S_t - \theta_2^P)e^{-\kappa_{22}^P(T-t)} - \kappa_{21}^P(L_t - \theta_1^P)\frac{e^{-\kappa_{11}^P(T-t)} - e^{-\kappa_{22}^P(T-t)}}{\kappa_{22}^P - \kappa_{11}^P} \\
&\quad + \kappa_{21}^P\kappa_{13}^P(C_t - \theta_3^P)\frac{e^{-\kappa_{33}^P(T-t)} - e^{-\kappa_{22}^P(T-t)}}{(\kappa_{11}^P - \kappa_{33}^P)(\kappa_{22}^P - \kappa_{33}^P)} - \kappa_{21}^P\kappa_{13}^P(C_t - \theta_3^P)\frac{e^{-\kappa_{11}^P(T-t)} - e^{-\kappa_{22}^P(T-t)}}{(\kappa_{11}^P - \kappa_{33}^P)(\kappa_{22}^P - \kappa_{11}^P)} \\
&\quad - \kappa_{23}^P(C_t - \theta_3^P)\frac{e^{-\kappa_{33}^P(T-t)} - e^{-\kappa_{22}^P(T-t)}}{\kappa_{22}^P - \kappa_{33}^P}.
\end{aligned}$$

In the zero-bound state, the expected short rate τ years ahead is given by

$$\begin{aligned}
E_t^P[r_{t+\tau}] &= 0 \cdot E_t^P\left[e^{-\int_t^{t+\tau}\eta_u du}\right] + E_t^P\left[\int_t^{t+\tau}\eta_s e^{-\int_t^s \eta_u du} r_{t+\tau} ds\right] \\
&= \int_t^{t+\tau} E_t^P\left[\eta_s e^{-\int_t^s \eta_u du} E_s^P[r_{t+\tau}]\right] ds.
\end{aligned}$$

Thus, we need the formula for $E_s^P[r_{t+\tau}]$ from the normal state to be able to calculate the involved conditional expectation. This is an affine function in the state variables:

$$E_s^P[r_{t+\tau}] = \overline{A}^{PE}(s, t+\tau) + \overline{B}_L^{PE}(s, t+\tau)L_s + \overline{B}_S^{PE}(s, t+\tau)S_s + \overline{B}_C^{PE}(s, t+\tau)C_s,$$

[34] The calculations leading to these results are available from the author upon request.

where

$$
\begin{aligned}
\overline{A}^{PE}(s,t+\tau) &= (1-e^{-\kappa_{11}^P(t+\tau-s)})\theta_1^P + \kappa_{21}^P \frac{e^{-\kappa_{11}^P(t+\tau-s)} - e^{-\kappa_{22}^P(t+\tau-s)}}{\kappa_{22}^P - \kappa_{11}^P}\theta_1^P + (1-e^{-\kappa_{22}^P(t+\tau-s)})\theta_2^P \\
&\quad + \kappa_{13}^P \frac{e^{-\kappa_{33}^P(t+\tau-s)} - e^{-\kappa_{11}^P(t+\tau-s)}}{\kappa_{11}^P - \kappa_{33}^P}\theta_3^P - \kappa_{21}^P\kappa_{13}^P \frac{e^{-\kappa_{33}^P(t+\tau-s)} - e^{-\kappa_{22}^P(t+\tau-s)}}{(\kappa_{11}^P - \kappa_{33}^P)(\kappa_{22}^P - \kappa_{33}^P)}\theta_3^P \\
&\quad + \kappa_{21}^P\kappa_{13}^P \frac{e^{-\kappa_{11}^P(t+\tau-s)} - e^{-\kappa_{22}^P(t+\tau-s)}}{(\kappa_{11}^P - \kappa_{33}^P)(\kappa_{22}^P - \kappa_{11}^P)}\theta_3^P + \kappa_{23}^P \frac{e^{-\kappa_{33}^P(t+\tau-s)} - e^{-\kappa_{22}^P(t+\tau-s)}}{\kappa_{22}^P - \kappa_{33}^P}\theta_3^P, \\
\overline{B}_L^{PE}(s,t+\tau) &= e^{-\kappa_{11}^P(t+\tau-s)} - \kappa_{21}^P \frac{e^{-\kappa_{11}^P(t+\tau-s)} - e^{-\kappa_{22}^P(t+\tau-s)}}{\kappa_{22}^P - \kappa_{11}^P}, \\
\overline{B}_S^{PE}(s,t+\tau) &= e^{-\kappa_{22}^P(t+\tau-s)}, \\
\overline{B}_C^{PE}(s,t+\tau) &= -\kappa_{13}^P \frac{e^{-\kappa_{33}^P(t+\tau-s)} - e^{-\kappa_{11}^P(t+\tau-s)}}{\kappa_{11}^P - \kappa_{33}^P} + \kappa_{21}^P\kappa_{13}^P \frac{e^{-\kappa_{33}^P(t+\tau-s)} - e^{-\kappa_{22}^P(t+\tau-s)}}{(\kappa_{11}^P - \kappa_{33}^P)(\kappa_{22}^P - \kappa_{33}^P)} \\
&\quad - \kappa_{21}^P\kappa_{13}^P \frac{e^{-\kappa_{11}^P(t+\tau-s)} - e^{-\kappa_{22}^P(t+\tau-s)}}{(\kappa_{11}^P - \kappa_{33}^P)(\kappa_{22}^P - \kappa_{11}^P)} - \kappa_{23}^P \frac{e^{-\kappa_{33}^P(t+\tau-s)} - e^{-\kappa_{22}^P(t+\tau-s)}}{\kappa_{22}^P - \kappa_{33}^P}.
\end{aligned}
$$

Now, we are interested in the following expectation

$$
\begin{aligned}
& E_t^P\Big[\eta_s e^{-\int_t^s \eta_u du} E_s^P[r_{t+\tau}]\Big] \\
= \; & E_t^P\Big[\eta_s e^{-\int_t^s \eta_u du}\Big(\overline{A}^{PE}(s,t+\tau) + \overline{B}_L^{PE}(s,t+\tau)L_s + \overline{B}_S^{PE}(s,t+\tau)S_s + \overline{B}_C^{PE}(s,t+\tau)C_s\Big)\Big].
\end{aligned}
$$

Towards this goal, Christensen (2007) has the following result.

Proposition 2:

Let the state variables X_t be described by an affine diffusion process

$$dX_t = [\mu^0 + \mu^1 X_t]dt + \Sigma D(X_t)dW_t \tag{10}$$

defined on a set $M \subset \mathbf{R}^n$. Here, $D : M \to \mathbf{R}^{n\times n}$ is assumed to have the following diagonal structure

$$
D(X_t) = \begin{pmatrix}
\sqrt{\gamma^1 + \delta_1^1 X_t^1 + \ldots + \delta_n^1 X_t^n} & \ldots & 0 \\
\vdots & \ddots & \vdots \\
0 & \ldots & \sqrt{\gamma^n + \delta_1^n X_t^1 + \ldots + \delta_n^n X_t^n}
\end{pmatrix}.
$$

To simplify notation below, γ and δ are defined as

$$
\gamma = \begin{pmatrix} \gamma^1 \\ \vdots \\ \gamma^n \end{pmatrix} \quad \text{and} \quad \delta = \begin{pmatrix} \delta_1^1 & \ldots & \delta_n^1 \\ \vdots & \ddots & \vdots \\ \delta_1^n & \ldots & \delta_n^n \end{pmatrix}.
$$

In addition, assume the discount process to be affine in the state variables

$$R(X_t) = \rho_0 + \rho_1' X_t.$$

Then the expectation

$$G(X_t,t,T) = E\Big[e^{-\int_t^T R(X_s)ds} e^{\overline{B}' X_T + \overline{C}}\big[X_T'\overline{D}X_T + \overline{E}'X_T + \overline{F}\big]\Big|\mathcal{F}_t\Big],$$

where $\overline{D} \in \mathbf{R}^{n\times n}$, $\overline{B}, \overline{E} \in \mathbf{R}^n$, and $\overline{C} \in \mathbf{R}$, is given by

$$G(X_t, t, T) = \exp\big(B(t,T)'X_t + C(t,T)\big)\big[X_t'D(t,T)X_t + E(t,T)'X_t + F(t,T)\big],$$

if the following conditions are satisfied.

(i). There exists a unique solution X_t for the stochastic differential equation (10) for all $0 \le t \le T$.

(ii). There exist functions $B(t,T)$, $C(t,T)$, $D(t,T)$, $E(t,T)$, and $F(t,T)$ which are the unique solutions for the following system of first-order ordinary differential equations (ODE)[35]

$$\begin{aligned}
\frac{dB(t,T)}{dt} &= \rho_1 - (\mu^1)'B(t,T) - \frac{1}{2}\sum_{j=1}^{n}(\Sigma' B(t,T)B(t,T)'\Sigma)_{j,j}(\delta^j)', \quad B(T,T) = \overline{B},\\
\frac{dC(t,T)}{dt} &= \rho_0 - B(t,T)'\mu^0 - \frac{1}{2}\sum_{j=1}^{n}(\Sigma' B(t,T)B(t,T)'\Sigma)_{j,j}\gamma^j, \quad C(T,T) = \overline{C},\\
\frac{dD(t,T)}{dt} &= -(\mu^1)'D(t,T) - D(t,T)\mu^1 - \sum_{j=1}^{n}(\Sigma' B(t,T))_j(D(t,T)\Sigma)_{\cdot,j}\delta^j\\
&\quad - \sum_{j=1}^{n}(\Sigma' B(t,T))_j(D(t,T)'\Sigma)_{\cdot,j}\delta^j, \quad D(T,T) = \overline{D},\\
\frac{dE(t,T)}{dt} &= -(\mu^1)'E(t,T) - D(t,T)'\mu^0 - D(t,T)\mu^0 - \sum_{j=1}^{n}(\Sigma' B(t,T)E(t,T)'\Sigma)_{j,j}(\delta^j)'\\
&\quad - \sum_{j=1}^{n}(\Sigma' D(t,T)\Sigma)_{j,j}(\delta^j)' - \sum_{j=1}^{n}(\Sigma' B(t,T))_j(D(t,T)\Sigma)_{\cdot,j}\gamma^j\\
&\quad - \sum_{j=1}^{n}(\Sigma' B(t,T))_j(D(t,T)'\Sigma)_{\cdot,j}\gamma^j, \quad E(T,T) = \overline{E},\\
\frac{dF(t,T)}{dt} &= -E(t,T)'\mu^0 - \sum_{j=1}^{n}(\Sigma' D(t,T)\Sigma)_{j,j}\gamma^j - \sum_{j=1}^{n}(\Sigma' B(t,T)E(t,T)'\Sigma)_{j,j}\gamma^j, \quad F(T,T) = \overline{F},
\end{aligned}$$

(iii). The following technical conditions are met

(a) $E[|\Phi_T|] < \infty$,

(b) $E\Big[\big(\int_0^T \eta_t\eta_t' dt\big)^{1/2}\Big] < \infty$ for $\eta_t = \big(\Phi_t B(t,T)' + \Psi_t[E(t,T)' + X_t'(D(t,T) + D(t,T)')]\big)\Sigma D$,

where $\Phi_t = e^{-\int_0^t r(X_s,s)ds}e^{B(t,T)'X_t + C(t,T)}[X_t'D(t,T)X_t + E(t,T)'X_t + F(t,T)]$ and
$\Psi_t = e^{-\int_0^t r(X_s,s)ds}e^{B(t,T)'X_t + C(t,T)}$ for all $0 \le t \le T$.

This proposition implies that it only requires the solution of a system of ODEs to calculate the expectations appearing in the definition of the term premium in the zero-bound state. In this paper, this is done by standard fourth-order Runge Kutta methods.

In the zero-bound state, the joint P-dynamics of the state variables preferred by the Akaike information

[35] Here, δ^j denotes the jth row of the δ-matrix.

criterion are given by

$$\begin{pmatrix} dL_t \\ dS_t \\ dC_t \\ d\eta_t \end{pmatrix} = \begin{pmatrix} \kappa_{11}^P & 0 & \kappa_{13}^P & 0 \\ \kappa_{21}^P & \kappa_{22}^P & \kappa_{23}^P & \kappa_{24}^P \\ 0 & 0 & \kappa_{33}^P & \kappa_{34}^P \\ 0 & 0 & 0 & \kappa_{44}^P \end{pmatrix} \left[\begin{pmatrix} \theta_1^P \\ \theta_2^P \\ \theta_3^P \\ \theta_4^P \end{pmatrix} - \begin{pmatrix} L_t \\ S_t \\ C_t \\ \eta_t \end{pmatrix} \right] dt$$
$$+ \begin{pmatrix} \sigma_L & 0 & 0 & 0 \\ 0 & \sigma_S & 0 & 0 \\ 0 & 0 & \sigma_C & 0 \\ 0 & 0 & 0 & \sigma_\eta \end{pmatrix} \begin{pmatrix} \sqrt{1} & 0 & 0 & 0 \\ 0 & \sqrt{1} & 0 & 0 \\ 0 & 0 & \sqrt{1} & 0 \\ 0 & 0 & 0 & \sqrt{\eta_t} \end{pmatrix} \begin{pmatrix} dW_t^{L,P} \\ dW_t^{S,P} \\ dW_t^{C,P} \\ dW_t^{\eta,P} \end{pmatrix}.$$

In this case, the vectors and matrices describing the P-dynamics of the state variables and appearing in the system of ODEs in Proposition 2 are given by:

$$\rho_0 = 0, \quad \rho_1 = \begin{pmatrix} 0 \\ 0 \\ 0 \\ 1 \end{pmatrix}, \quad \mu^0 = \begin{pmatrix} \kappa_{11}^P & 0 & \kappa_{13}^P & 0 \\ \kappa_{21}^P & \kappa_{22}^P & \kappa_{23}^P & \kappa_{24}^P \\ 0 & 0 & \kappa_{33}^P & \kappa_{34}^P \\ 0 & 0 & 0 & \kappa_{44}^P \end{pmatrix} \begin{pmatrix} \theta_1^P \\ \theta_2^P \\ \theta_3^P \\ \theta_4^P \end{pmatrix}, \quad \mu^1 = - \begin{pmatrix} \kappa_{11}^P & 0 & \kappa_{13}^P & 0 \\ \kappa_{21}^P & \kappa_{22}^P & \kappa_{23}^P & \kappa_{24}^P \\ 0 & 0 & \kappa_{33}^P & \kappa_{34}^P \\ 0 & 0 & 0 & \kappa_{44}^P \end{pmatrix},$$

$$\Sigma = \begin{pmatrix} \sigma_L & 0 & 0 & 0 \\ 0 & \sigma_S & 0 & 0 \\ 0 & 0 & \sigma_C & 0 \\ 0 & 0 & 0 & \sigma_\eta \end{pmatrix}, \quad \gamma = \begin{pmatrix} 1 \\ 1 \\ 1 \\ 0 \end{pmatrix}, \quad \text{and} \quad \delta = \begin{pmatrix} 0 & 0 & 0 & 0 \\ 0 & 0 & 0 & 0 \\ 0 & 0 & 0 & 0 \\ 0 & 0 & 0 & 1 \end{pmatrix}.$$

Finally, the boundary conditions in the system of ODEs in Proposition 2 are given by:

$$\overline{B} = \begin{pmatrix} 0 \\ 0 \\ 0 \\ 0 \end{pmatrix}, \quad \overline{C} = 0, \quad \overline{D} = \begin{pmatrix} 0 & 0 & 0 & \frac{1}{2}\overline{B}_L^{PE}(s, t+\tau) \\ 0 & 0 & 0 & \frac{1}{2}\overline{B}_S^{PE}(s, t+\tau) \\ 0 & 0 & 0 & \frac{1}{2}\overline{B}_C^{PE}(s, t+\tau) \\ \frac{1}{2}\overline{B}_L^{PE}(s, t+\tau) & \frac{1}{2}\overline{B}_S^{PE}(s, t+\tau) & \frac{1}{2}\overline{B}_C^{PE}(s, t+\tau) & 0 \end{pmatrix},$$

$$\overline{E} = \begin{pmatrix} 0 \\ 0 \\ 0 \\ \overline{A}^{PE}(s, t+\tau) \end{pmatrix}, \quad \overline{F} = 0.$$

Now, denote the solution to the system of ODEs in Proposition 2 by $B^{PE}(t, s, t+\tau)$, $C^{PE}(t, s, t+\tau)$, $D^{PE}(t, s, t+\tau)$, $E^{PE}(t, s, t+\tau)$, and $F^{PE}(t, s, t+\tau)$, and it follows that

$$\begin{aligned} & E_t^P\left[\eta_s e^{-\int_t^s \eta_u du} E_s^P[r_{t+\tau}]\right] \\ = \; & E_t^P\left[\eta_s e^{-\int_t^s \eta_u du}\left(\overline{A}^{PE}(s, t+\tau) + \overline{B}_L^{PE}(s, t+\tau)L_s + \overline{B}_S^{PE}(s, t+\tau)S_s + \overline{B}_C^{PE}(s, t+\tau)C_s\right)\right] \\ = \; & \exp\left(B^{PE}(t, s, t+\tau)'X_t + C^{PE}(t, s, t+\tau)\right)\left[X_t' D^{PE}(t, s, t+\tau)X_t + E^{PE}(t, s, t+\tau)'X_t + F^{PE}(t, s, t+\tau)\right]. \end{aligned}$$

Thus, the expected short rate in the zero-bound state is given by

$$\begin{aligned} E_t^P[r_{t+\tau}] &= \int_t^{t+\tau} E_t^P\Big[\eta_s e^{-\int_t^s \eta_u du} E_s^P[r_{t+\tau}]\Big] ds \\ &= \int_t^{t+\tau} \exp\Big(B^{PE}(t,s,t+\tau)' X_t + C^{PE}(t,s,t+\tau)\Big) \\ &\qquad \times \Big[X_t' D^{PE}(t,s,t+\tau) X_t + E^{PE}(t,s,t+\tau)' X_t + F^{PE}(t,s,t+\tau)\Big] ds. \end{aligned}$$

Appendix C: Term Premiums in the Regime-Switching Model

In general, the term premium part of the yield on a zero coupon bond with maturity in τ years is defined as

$$TP_t(\tau) = y(t,t+\tau) - \frac{1}{\tau}\int_t^{t+\tau} E_t^P[r_s] ds.$$

In the normal state, the term premium takes its usual form

$$TP_t^N(\tau) = y^N(t,t+\tau) - \frac{1}{\tau}\int_t^{t+\tau} E_t^P[r_s] ds, \tag{11}$$

where the instantaneous rate is the sum of the first two factors

$$r_t = L_t + S_t.$$

In the specification of the regime-switching model preferred according to the AIC, the P-dynamics in the normal state are given by

$$\begin{pmatrix} dL_t \\ dS_t \\ dC_t \end{pmatrix} = \begin{pmatrix} \kappa_{11}^P & 0 & \kappa_{13}^P \\ \kappa_{21}^P & \kappa_{22}^P & \kappa_{23}^P \\ 0 & 0 & \kappa_{33}^P \end{pmatrix} \left[\begin{pmatrix} \theta_1^P \\ \theta_2^P \\ \theta_3^P \end{pmatrix} - \begin{pmatrix} L_t \\ S_t \\ C_t \end{pmatrix} \right] dt + \begin{pmatrix} \sigma_L & 0 & 0 \\ 0 & \sigma_S & 0 \\ 0 & 0 & \sigma_C \end{pmatrix} \begin{pmatrix} dW_t^{L,P} \\ dW_t^{S,P} \\ dW_t^{C,P} \end{pmatrix}.$$

From Appendix B it follows that the conditional mean of L_t and S_t are given by

$$\begin{aligned} E_t^P[L_T] &= \theta_1^P + (L_t - \theta_1^P) e^{-\kappa_{11}^P (T-t)} - \kappa_{13}^P (C_t - \theta_3^P) \frac{e^{-\kappa_{33}^P (T-t)} - e^{-\kappa_{11}^P (T-t)}}{\kappa_{11}^P - \kappa_{33}^P}, \\ E_t^P[S_T] &= \theta_2^P + (S_t - \theta_2^P) e^{-\kappa_{22}^P (T-t)} - \kappa_{21}^P (L_t - \theta_1^P) \frac{e^{-\kappa_{11}^P (T-t)} - e^{-\kappa_{22}^P (T-t)}}{\kappa_{22}^P - \kappa_{11}^P} \\ &\quad + \kappa_{21}^P \kappa_{13}^P (C_t - \theta_3^P) \frac{e^{-\kappa_{33}^P (T-t)} - e^{-\kappa_{22}^P (T-t)}}{(\kappa_{11}^P - \kappa_{33}^P)(\kappa_{22}^P - \kappa_{33}^P)} - \kappa_{21}^P \kappa_{13}^P (C_t - \theta_3^P) \frac{e^{-\kappa_{11}^P (T-t)} - e^{-\kappa_{22}^P (T-t)}}{(\kappa_{11}^P - \kappa_{33}^P)(\kappa_{22}^P - \kappa_{11}^P)} \\ &\quad - \kappa_{23}^P (C_t - \theta_3^P) \frac{e^{-\kappa_{33}^P (T-t)} - e^{-\kappa_{22}^P (T-t)}}{\kappa_{22}^P - \kappa_{33}^P}. \end{aligned}$$

Now, the integral of the instantaneous rate over the interval from t to $t+\tau$ is[36]

$$\begin{aligned}
\int_t^{t+\tau} E_t^P[r_s]ds &= \frac{1-e^{-\kappa_{11}^P\tau}}{\kappa_{11}^P}L_t - \frac{\kappa_{21}^P}{\kappa_{22}^P-\kappa_{11}^P}\Big(\frac{1-e^{-\kappa_{11}^P\tau}}{\kappa_{11}^P} - \frac{1-e^{-\kappa_{22}^P\tau}}{\kappa_{22}^P}\Big)L_t + \frac{1-e^{-\kappa_{22}^P\tau}}{\kappa_{22}^P}S_t \\
&\quad - \frac{\kappa_{13}^P}{\kappa_{11}^P-\kappa_{33}^P}\Big(\frac{1-e^{-\kappa_{33}^P\tau}}{\kappa_{33}^P} - \frac{1-e^{-\kappa_{11}^P\tau}}{\kappa_{11}^P}\Big)C_t - \frac{\kappa_{23}^P}{\kappa_{22}^P-\kappa_{33}^P}\Big(\frac{1-e^{-\kappa_{33}^P\tau}}{\kappa_{33}^P} - \frac{1-e^{-\kappa_{22}^P\tau}}{\kappa_{22}^P}\Big)C_t \\
&\quad + \frac{\kappa_{21}^P\kappa_{13}^P}{(\kappa_{11}^P-\kappa_{33}^P)(\kappa_{22}^P-\kappa_{33}^P)}\Big(\frac{1-e^{-\kappa_{33}^P\tau}}{\kappa_{33}^P} - \frac{1-e^{-\kappa_{22}^P\tau}}{\kappa_{22}^P}\Big)C_t \\
&\quad - \frac{\kappa_{21}^P\kappa_{13}^P}{(\kappa_{11}^P-\kappa_{33}^P)(\kappa_{22}^P-\kappa_{11}^P)}\Big(\frac{1-e^{-\kappa_{11}^P\tau}}{\kappa_{11}^P} - \frac{1-e^{-\kappa_{22}^P\tau}}{\kappa_{22}^P}\Big)C_t \\
&\quad + (\theta_1^P+\theta_2^P)\tau - \frac{1-e^{-\kappa_{11}^P\tau}}{\kappa_{11}^P}\theta_1^P + \frac{\kappa_{21}^P}{\kappa_{22}^P-\kappa_{11}^P}\Big(\frac{1-e^{-\kappa_{11}^P\tau}}{\kappa_{11}^P} - \frac{1-e^{-\kappa_{22}^P\tau}}{\kappa_{22}^P}\Big)\theta_1^P - \frac{1-e^{-\kappa_{22}^P\tau}}{\kappa_{22}^P}\theta_2^P \\
&\quad + \frac{\kappa_{13}^P}{\kappa_{11}^P-\kappa_{33}^P}\Big(\frac{1-e^{-\kappa_{33}^P\tau}}{\kappa_{33}^P} - \frac{1-e^{-\kappa_{11}^P\tau}}{\kappa_{11}^P}\Big)\theta_3^P + \frac{\kappa_{23}^P}{\kappa_{22}^P-\kappa_{33}^P}\Big(\frac{1-e^{-\kappa_{33}^P\tau}}{\kappa_{33}^P} - \frac{1-e^{-\kappa_{22}^P\tau}}{\kappa_{22}^P}\Big)\theta_3^P \\
&\quad - \frac{\kappa_{21}^P\kappa_{13}^P}{(\kappa_{11}^P-\kappa_{33}^P)(\kappa_{22}^P-\kappa_{33}^P)}\Big(\frac{1-e^{-\kappa_{33}^P\tau}}{\kappa_{33}^P} - \frac{1-e^{-\kappa_{22}^P\tau}}{\kappa_{22}^P}\Big)\theta_3^P \\
&\quad + \frac{\kappa_{21}^P\kappa_{13}^P}{(\kappa_{11}^P-\kappa_{33}^P)(\kappa_{22}^P-\kappa_{11}^P)}\Big(\frac{1-e^{-\kappa_{11}^P\tau}}{\kappa_{11}^P} - \frac{1-e^{-\kappa_{22}^P\tau}}{\kappa_{22}^P}\Big)\theta_3^P.
\end{aligned}$$

In the zero-bound state, the formula for the term premium is given by

$$\begin{aligned}
TP_t^Z(\tau) &= y^Z(t,t+\tau) - \frac{1}{\tau}\Big(0\cdot E_t^P[e^{-\int_t^{t+\tau}\eta_u du}] + E_t^P[\int_t^{t+\tau}\eta_s e^{-\int_t^s \eta_u du}\int_s^{t+\tau} r_u du ds]\Big) \\
&= y^Z(t,t+\tau) - \frac{1}{\tau}\int_t^{t+\tau} E_t^P\Big[\eta_s e^{-\int_t^s \eta_u du}E_s^P[\int_s^{t+\tau} r_u du]\Big]ds.
\end{aligned}$$

Thus, we need the formula for $E_s^P[\int_s^{t+\tau} r_u du]$ from the normal state to be able to calculate the involved conditional expectation. This is an affine function in the state variables:

$$E_s^P[\int_s^{t+\tau} r_u du] = \overline{A}^{TP}(s,t+\tau) + \overline{B}_L^{TP}(s,t+\tau)L_s + \overline{B}_S^{TP}(s,t+\tau)S_s + \overline{B}_C^{TP}(s,t+\tau)C_s,$$

[36]The calculations leading to these results are available from the author upon request.

where

$$
\begin{aligned}
\overline{A}^{TP}(s,t+\tau) &= (\theta_1^P+\theta_2^P)(t+\tau-s)-\frac{1-e^{-\kappa_{11}^P(t+\tau-s)}}{\kappa_{11}^P}\theta_1^P \\
&\quad+\frac{\kappa_{21}^P}{\kappa_{22}^P-\kappa_{11}^P}\Big(\frac{1-e^{-\kappa_{11}^P(t+\tau-s)}}{\kappa_{11}^P}-\frac{1-e^{-\kappa_{22}^P(t+\tau-s)}}{\kappa_{22}^P}\Big)\theta_1^P-\frac{1-e^{-\kappa_{22}^P(t+\tau-s)}}{\kappa_{22}^P}\theta_2^P \\
&\quad+\frac{\kappa_{13}^P}{\kappa_{11}^P-\kappa_{33}^P}\Big(\frac{1-e^{-\kappa_{33}^P(t+\tau-s)}}{\kappa_{33}^P}-\frac{1-e^{-\kappa_{11}^P(t+\tau-s)}}{\kappa_{11}^P}\Big)\theta_3^P \\
&\quad+\frac{\kappa_{23}^P}{\kappa_{22}^P-\kappa_{33}^P}\Big(\frac{1-e^{-\kappa_{33}^P(t+\tau-s)}}{\kappa_{33}^P}-\frac{1-e^{-\kappa_{22}^P(t+\tau-s)}}{\kappa_{22}^P}\Big)\theta_3^P \\
&\quad-\frac{\kappa_{21}^P\kappa_{13}^P}{(\kappa_{11}^P-\kappa_{33}^P)(\kappa_{22}^P-\kappa_{33}^P)}\Big(\frac{1-e^{-\kappa_{33}^P(t+\tau-s)}}{\kappa_{33}^P}-\frac{1-e^{-\kappa_{22}^P(t+\tau-s)}}{\kappa_{22}^P}\Big)\theta_3^P \\
&\quad+\frac{\kappa_{21}^P\kappa_{13}^P}{(\kappa_{11}^P-\kappa_{33}^P)(\kappa_{22}^P-\kappa_{11}^P)}\Big(\frac{1-e^{-\kappa_{11}^P(t+\tau-s)}}{\kappa_{11}^P}-\frac{1-e^{-\kappa_{22}^P(t+\tau-s)}}{\kappa_{22}^P}\Big)\theta_3^P, \\
\overline{B}_L^{TP}(s,t+\tau) &= \frac{1-e^{-\kappa_{11}^P(t+\tau-s)}}{\kappa_{11}^P}-\frac{\kappa_{21}^P}{\kappa_{22}^P-\kappa_{11}^P}\Big(\frac{1-e^{-\kappa_{11}^P(t+\tau-s)}}{\kappa_{11}^P}-\frac{1-e^{-\kappa_{22}^P(t+\tau-s)}}{\kappa_{22}^P}\Big), \\
\overline{B}_S^{TP}(s,t+\tau) &= \frac{1-e^{-\kappa_{22}^P(t+\tau-s)}}{\kappa_{22}^P}, \\
\overline{B}_C^{TP}(s,t+\tau) &= -\frac{\kappa_{13}^P}{\kappa_{11}^P-\kappa_{33}^P}\Big(\frac{1-e^{-\kappa_{33}^P(t+\tau-s)}}{\kappa_{33}^P}-\frac{1-e^{-\kappa_{11}^P(t+\tau-s)}}{\kappa_{11}^P}\Big) \\
&\quad-\frac{\kappa_{23}^P}{\kappa_{22}^P-\kappa_{33}^P}\Big(\frac{1-e^{-\kappa_{33}^P(t+\tau-s)}}{\kappa_{33}^P}-\frac{1-e^{-\kappa_{22}^P(t+\tau-s)}}{\kappa_{22}^P}\Big) \\
&\quad+\frac{\kappa_{21}^P\kappa_{13}^P}{(\kappa_{11}^P-\kappa_{33}^P)(\kappa_{22}^P-\kappa_{33}^P)}\Big(\frac{1-e^{-\kappa_{33}^P(t+\tau-s)}}{\kappa_{33}^P}-\frac{1-e^{-\kappa_{22}^P(t+\tau-s)}}{\kappa_{22}^P}\Big) \\
&\quad-\frac{\kappa_{21}^P\kappa_{13}^P}{(\kappa_{11}^P-\kappa_{33}^P)(\kappa_{22}^P-\kappa_{11}^P)}\Big(\frac{1-e^{-\kappa_{11}^P(t+\tau-s)}}{\kappa_{11}^P}-\frac{1-e^{-\kappa_{22}^P(t+\tau-s)}}{\kappa_{22}^P}\Big).
\end{aligned}
$$

Now, we are interested in the following expectation

$$
\begin{aligned}
& E_t^P\Big[\eta_s e^{-\int_t^s \eta_u du}E_s^P[\int_s^{t+\tau} r_u du]\Big] \\
= \;& E_t^P\Big[\eta_s e^{-\int_t^s \eta_u du}\Big(\overline{A}^{TP}(s,t+\tau)+\overline{B}_L^{TP}(s,t+\tau)L_s+\overline{B}_S^{TP}(s,t+\tau)S_s+\overline{B}_C^{TP}(s,t+\tau)C_s\Big)\Big],
\end{aligned}
$$

where Proposition 2 in Appendix B can again be applied.

In the zero-bound state, the joint P-dynamics of the state variables remain as described in Appendix B. Thus, the vectors and matrices describing the P-dynamics of the state variables and appearing in the system of ODEs in Proposition 2 remain given by:

$$
\rho_0=0,\quad \rho_1=\begin{pmatrix}0\\0\\0\\1\end{pmatrix},\quad \mu^0=\begin{pmatrix}\kappa_{11}^P & 0 & \kappa_{13}^P & 0\\ \kappa_{21}^P & \kappa_{22}^P & \kappa_{23}^P & \kappa_{24}^P\\ 0 & 0 & \kappa_{33}^P & \kappa_{34}^P\\ 0 & 0 & 0 & \kappa_{44}^P\end{pmatrix}\begin{pmatrix}\theta_1^P\\ \theta_2^P\\ \theta_3^P\\ \theta_4^P\end{pmatrix},\quad \mu^1=-\begin{pmatrix}\kappa_{11}^P & 0 & \kappa_{13}^P & 0\\ \kappa_{21}^P & \kappa_{22}^P & \kappa_{23}^P & \kappa_{24}^P\\ 0 & 0 & \kappa_{33}^P & \kappa_{34}^P\\ 0 & 0 & 0 & \kappa_{44}^P\end{pmatrix},
$$

$$
\Sigma=\begin{pmatrix}\sigma_L & 0 & 0 & 0\\ 0 & \sigma_S & 0 & 0\\ 0 & 0 & \sigma_C & 0\\ 0 & 0 & 0 & \sigma_\eta\end{pmatrix},\quad \gamma=\begin{pmatrix}1\\1\\1\\0\end{pmatrix},\quad \text{and}\quad \delta=\begin{pmatrix}0&0&0&0\\0&0&0&0\\0&0&0&0\\0&0&0&1\end{pmatrix}.
$$

Finally, the boundary conditions in the system of ODEs in Proposition 2 are given by:

$$\overline{B} = \begin{pmatrix} 0 \\ 0 \\ 0 \\ 0 \end{pmatrix}, \quad \overline{C} = 0, \quad \overline{D} = \begin{pmatrix} 0 & 0 & 0 & \frac{1}{2}\overline{B}_L^{TP}(s,t+\tau) \\ 0 & 0 & 0 & \frac{1}{2}\overline{B}_S^{TP}(s,t+\tau) \\ 0 & 0 & 0 & \frac{1}{2}\overline{B}_C^{TP}(s,t+\tau) \\ \frac{1}{2}\overline{B}_L^{TP}(s,t+\tau) & \frac{1}{2}\overline{B}_S^{TP}(s,t+\tau) & \frac{1}{2}\overline{B}_C^{TP}(s,t+\tau) & 0 \end{pmatrix},$$

$$\overline{E} = \begin{pmatrix} 0 \\ 0 \\ 0 \\ \overline{A}^{TP}(s,t+\tau) \end{pmatrix}, \quad \overline{F} = 0.$$

Now, denote the solution to the system of ODEs in Proposition 1 by $B^{TP}(t,s,t+\tau)$, $C^{TP}(t,s,t+\tau)$, $D^{TP}(t,s,t+\tau)$, $E^{TP}(t,s,t+\tau)$, and $F^{TP}(t,s,t+\tau)$, and it follows that

$$\begin{aligned} & E_t^P\Big[\eta_s e^{-\int_t^s \eta_u du} E_s^P[\int_s^{t+\tau} r_u du]\Big] \\ = \; & E_t^P\Big[\eta_s e^{-\int_t^s \eta_u du}\Big(\overline{A}^{TP}(s,t+\tau) + \overline{B}_L^{TP}(s,t+\tau)L_s + \overline{B}_S^{TP}(s,t+\tau)S_s + \overline{B}_C^{TP}(s,t+\tau)C_s\Big)\Big] \\ = \; & \exp\Big(B^{TP}(t,s,t+\tau)'X_t + C^{TP}(t,s,t+\tau)\Big)\Big[X_t' D^{TP}(t,s,t+\tau)X_t + E^{TP}(t,s,t+\tau)'X_t + F^{TP}(t,s,t+\tau)\Big]. \end{aligned}$$

Thus, the term premium in the zero-bound state is calculated as

$$\begin{aligned} TP_t^Z(\tau) &= y^Z(t,t+\tau) - \frac{1}{\tau}\int_t^{t+\tau} E_t^P\Big[\eta_s e^{-\int_t^s \eta_u du} E_s^P[\int_s^{t+\tau} r_u du]\Big] ds \\ &= y^Z(t,t+\tau) - \frac{1}{\tau}\int_t^{t+\tau} \exp\Big(B^{TP}(t,s,t+\tau)'X_t + C^{TP}(t,s,t+\tau)\Big) \\ &\qquad \times\Big[X_t' D^{TP}(t,s,t+\tau)X_t + E^{TP}(t,s,t+\tau)'X_t + F^{TP}(t,s,t+\tau)\Big] ds. \end{aligned}$$

References

Andersen, T., T. Bollerslev, F. Diebold, and Labys, P., 2003, "Modeling and Forecasting Realized Volatility," *Econometrica*, Vol. 71, 579-626.

Andersen, Torben G. and Luca Benzoni, 2010, "Do Bonds Span Volatility Risk in the U.S. Treasury Market? A Specification Test for Affine Term Structure Models," *Journal of Finance*, Vol. 65, No. 2, 603-653.

Bauer, Michael D. and Glenn D. Rudebusch, 2013a, "Monetary Policy Expectations at the Zero Lower Bound," Working Paper 2013-18, Federal Reserve Bank of San Francisco.

Bauer, Michael D. and Glenn D. Rudebusch, 2013b, "The Signaling Channel for Federal Reserve Bond Purchases," *International Journal of Central Banking*, forthcoming.

Bauer, Michael D., Glenn D. Rudebusch, and Jing (Cynthia) Wu, 2012, "Correcting Estimation Bias in Dynamic Term Structure Models," *Journal of Business and Economic Statistics*, Vol. 30, No. 3, 454-467.

Cheridito, Patrick, Damir Filipović, and Robert L. Kimmel, 2007, "Market Price of Risk Specifications for Affine Models: Theory and Evidence," *Journal of Financial Economics*, Vol. 83, 123-170.

Christensen, Jens H. E., 2007, "Default and Recovery Risk Modeling and Estimation," PhD Dissertation, PhD Series 18.2007, Department of Finance, Copenhagen Business School.

Christensen, Jens H. E., Francis X. Diebold, and Glenn D. Rudebusch, 2011, "The Affine Arbitrage-Free Class of Nelson-Siegel Term Structure Models," *Journal of Econometrics*, Vol. 164, pp. 4-20.

Christensen, Jens H. E., Jose A. Lopez, and Glenn D. Rudebusch, 2010, "Inflation Expectations and Risk Premiums in an Arbitrage-Free Model of Nominal and Real Bond Yields," *Journal of Money, Credit and Banking*, Supplement to Vol. 42, No. 6, 143-178.

Christensen, Jens H. E., Jose A. Lopez, and Glenn D. Rudebusch, 2012, "Pricing Deflation Risk with U.S. Treasury Yields," Working Paper 2012-07, Federal Reserve Bank of San Francisco.

Christensen, Jens H. E., Jose A. Lopez, and Glenn D. Rudebusch, 2013, "Can Spanned Term Structure Factors Drive Stochastic Yield Volatility?," Manuscript, Federal Reserve Bank of San Francisco.

Christensen, Jens H. E. and Glenn D. Rudebusch, 2012, "The Response of Interest Rates to U.S. and U.K. Quantitative Easing," *Economic Journal*, Vol. 122, F385-F414.

Collin-Dufresne, P., R.S. Goldstein, and C.S. Jones, 2009, "Can Interest Rate Volatility Be Extracted from the Cross-Section of Bond Yields?," *Journal of Financial Economics*, Vol. 94, 47-66.

Dai, Qiang, Ken Singleton, and Wei Yang, 2007, "Regime Shifts in a Dynamic Term Structure Model of U.S. Treasury Bond Yields," *Review of Financial Studies*, Vol. 20, 1669-1706.

Diebold, Francis X. and Glenn D. Rudebusch, 2013, *Yield Curve Modeling and Forecasting: The Dynamic Nelson-Siegel Approach*, Princeton, NJ: Princeton University Press.

Driessen, Joost, 2005, "Is Default Event Risk Priced in Corporate Bonds?" *Review of Financial Studies*, Vol. 18, No. 1, 165-195.

Duffee, Gregory R., 1999, "Estimating the Price of Default Risk," *Review of Financial Studies*, Vol. 12, 197-226.

Duffie, Darrell and David Lando, 2001, "Term Structures of Credit Spreads with Incomplete Accounting Information," *Econometrica*, Vol. 69, No. 3, 633-664.

Duffie, Darrell and Kenneth Singleton, 1999, "Modeling Term Structures of Defaultable Bonds," *Review of Financial Studies*, Vol. 12, No. 4, 687-720, 1999.

Feldhütter, Peter and David Lando, 2008, "Decomposing Swap Spreads," *Journal of Financial Economics*, Vol. 88, 375-405.

Fisher, Mark and Christian Gilles, 1996, "Term Premia in Exponential-Affine Models of the Term Structure," unpublished manuscript, Board of Governors of the Federal Reserve System.

Gürkaynak, Refet S., Brian Sack, and Jonathan H. Wright, 2007, "The U.S. Treasury Yield Curve: 1961 to the Present," *Journal of Monetary Economics*, Vol. 54, 2291-2304.

Harvey, A.C., 1989, *Forecasting, Structural Time Series Models and the Kalman Filter,* Cambridge: Cambridge University Press.

Jacobs, Kris and Lofti Karoui, 2009, "Conditional Volatility in Affine Term Structure Models: Evidence from Treasury and Swap Markets," *Journal of Financial Economics*, Vol. 91, 288-318.

Joslin, Scott, Kenneth Singleton, and Haoxiang Zhu, 2011, "A New Perspective on Gaussian DTSMs," *Review of Financial Studies*, Vol. 24, 926-970.

Kim, Don H. and Athanasios Orphanides, 2012, "Term Structure Estimation with Survey Data on Interest Rate Forecasts," *Journal of Financial and Quantitative Analysis*, Vol. 47, No. 1, 241-272.

Kim, Don H. and Kenneth J. Singleton, 2012, "Term Structure Models and the Zero Bound: An Empirical Investigation of Japanese Yields," *Journal of Econometrics*, Vol. 170, 32-49.

Kim, Don H. and Jonathan H. Wright, 2005, "An Arbitrage-Free Three-Factor Term Structure Model and the Recent Behavior of Long-Term Yields and Distant-Horizon Forward Rates," Working Paper Finance and Economics Discussion Series 2005-33, Board of Governors of the Federal Reserve System.

Koeda, Junko, 2013, "Endogenous Monetary Policy Shifts and the Term Structure: Evidence from Japanese Government Bond Yields," Manuscript, Faculty of Economics, University of Tokyo.

Krippner, Leo, 2013a, "A Theoretical Foundation for the Nelson and Siegel Class of Yield Curve Models," *Journal of Applied Econometrics*, forthcoming.

Krippner, Leo, 2013b, "A Tractable Framework for Zero Lower Bound Gaussian Term Structure Models," Discussion Paper 2013-02, Reserve Bank of New Zealand.

Litterman, R. and J. A. Scheinkman, 1991, "Common Factors Affecting Bond Returns," *Journal of Fixed Income*, Vol. 1, 62-74.

Nelson, Charles R. and Andrew F. Siegel, 1987, "Parsimonious Modeling of Yield Curves," *Journal of Business*, Vol. 60, 473-489.

Piazzesi, Monika, 2005, "Bond Yields and the Federal Reserve," *Journal of Political Economy*, Vol. 113, No. 2, 311-344.

Piazzesi, Monika and Eric T. Swanson, 2008, "Futures Prices as Risk-Adjusted Forecasts of Monetary Policy," *Journal of Monetary Economics*, Vol. 55, 677-691.

Swanson, Eric T. and John C. Williams, 2013, "Measuring the Effect of the Zero Lower Bound on Medium- and Longer-Term Interest Rates," Working Paper 2012-02, Federal Reserve Bank of San Francisco.

Wu, Jing Cynthia and Fan Dora Xia, 2013, "Measuring the Macroeconomic Impact of Monetary Policy at the Zero Lower Bound," Manuscript, Chicago Booth School of Business.